

Horseshoe Forests for High-Dimensional Causal Survival Analysis

Tijn Jacobs^{1*}, Wessel N. van Wieringen^{1,2}, Stéphanie L. van der Pas¹

29 July 2025

¹Department of Mathematics, Vrije Universiteit Amsterdam, Amsterdam, The Netherlands

²Department of Epidemiology and Data Science, Amsterdam University Medical Center, Amsterdam, The Netherlands

Abstract

We develop a Bayesian tree ensemble model to estimate heterogeneous treatment effects in censored survival data with high-dimensional covariates. Instead of imposing sparsity through the tree structure, we place a horseshoe prior directly on the step heights to achieve adaptive global-local shrinkage. This strategy allows flexible regularisation and reduces noise. We develop a reversible jump Gibbs sampler to accommodate the non-conjugate horseshoe prior within the tree ensemble framework. We show through extensive simulations that the method accurately estimates treatment effects in high-dimensional covariate spaces, at various sparsity levels, and under non-linear treatment effect functions. We further illustrate the practical utility of the proposed approach by a re-analysis of pancreatic ductal adenocarcinoma (PDAC) survival data from The Cancer Genome Atlas.

Keywords: Causal inference; heterogeneous treatment effects; survival analysis; high-dimensional; tree ensembles; shrinkage priors.

1 Introduction

Modelling heterogeneous treatment effects is challenging, especially with survival outcomes and high-dimensional covariates that may confound or modify treatment effects. We propose a Bayesian regression tree ensemble approach that uses a horseshoe prior to shrink tree step heights. This framework flexibly captures complex non-linear effects and interactions while providing adaptive shrinkage suited to high-dimensional causal inference with survival outcomes.

The conditional average treatment effect (CATE) quantifies how treatment effects vary across covariate profiles and is a central object in modelling heterogeneous treatment effects (Caron et al., 2022a). Estimating the CATE requires careful adjustment for confounding variables. This task becomes particularly challenging in high-dimensional settings with many covariates and complex interactions. In contrast, the average treatment effect (ATE) is low-dimensional and has been widely studied in high-dimensional contexts (Farrell, 2015; Antonelli et al., 2018; Antonelli and Cefalu, 2020; Ning et al., 2020; Antonelli et al., 2022). Researchers can

*Corresponding author: t.jacobs@vu.nl

treat high-dimensional components as nuisance terms when estimating the ATE, which simplifies inference. CATE estimation is fundamentally more difficult because the parameter of interest is high-dimensional and depends directly on covariates (Alaa and van der Schaar, 2018). Recent work has proposed flexible and robust methods for estimating heterogeneous treatment effects in high-dimensional covariate spaces (Powers et al., 2018; Fan et al., 2022; Shin and Antonelli, 2023). Despite this progress, a gap remains in extending these high-dimensional causal inference methods to survival data, where censoring and time-to-event outcomes introduce additional complexity.

Tree-based methods are widely used for causal inference in both frequentist and Bayesian frameworks. On the frequentist side, the causal forest algorithm of Wager and Athey (2018) extends the sample-splitting approach of Athey and Imbens (2016) to estimate heterogeneous treatment effects non-parametrically. This approach has been adapted to survival data by Cui et al. (2023). In the Bayesian setting, the Bayesian causal forest approach of Hahn et al. (2020) extends earlier work by Hill (2011). Hill applied Bayesian additive regression trees (BART) (Chipman et al., 2010) to estimate treatment effect heterogeneity. BART-based methods have demonstrated strong empirical performance and often outperform alternative estimators in benchmarking studies (Dorie et al., 2019; Thal and Finucane, 2023). Researchers have adapted these models to survival data to estimate conditional average treatment effects (Bonato et al., 2011; Henderson et al., 2020; Hu et al., 2023; Sun and Song, 2025). Recent work shows that AFT-BART (Henderson et al., 2020) outperforms other causal machine learning approaches in survival settings (Hu et al., 2021).

We adapt Bayesian additive regression trees to high-dimensional data by placing a global-local shrinkage prior on the step heights. In the original BART formulation, regularisation is imposed primarily through constraints on the tree structure, such as limiting tree depth or controlling the likelihood of node splits (Chipman et al., 2010). More recent extensions, such as the Dirichlet additive regression trees (DART) of Linero (2018), introduced Dirichlet priors on splitting proportions to encourage sparsity in the covariate space. Caron et al. (2022b) further extended this idea to causal inference. Our approach departs from this line of work by shifting the focus of regularisation away from the tree structure and onto the leaf node parameters. This approach preserves the flexibility of BART to model complex non-linear relationships. At the same time, it introduces adaptive shrinkage that suits high-dimensional causal inference. Rather than enforcing exact sparsity, our method retains all covariates and shrinks their influence based on data support. This reduces the risk of omitting confounders and improves robustness in observational settings.

Causal inference typically relies on the *unconfoundedness* assumption to identify treatment effects from observational data (Imbens and Rubin, 2015). It requires that, conditional on observed covariates, treatment assignment is independent of the potential outcomes:

$$T(a) \perp\!\!\!\perp A \mid X = x \quad \text{for } a \in \{0, 1\}. \quad (1)$$

Valid causal inference is possible by adjusting for the relevant covariates if this condition holds. Violating unconfoundedness may lead to biased estimates (Chernozhukov et al., 2022). In high-dimensional settings, adjustment becomes challenging: methods that remove covariates from the model may omit important confounders. We regularise the model using a continuous shrinkage prior. This approach retains covariates in the model that are needed for confounding adjustment.

Global-local shrinkage priors provide a fully Bayesian and computationally attractive alternative to exact sparsity-inducing methods (e.g. Mitchell and Beauchamp (1988) and Liu et al. (2021)). Originally developed for sparse regression problems (Carvalho et al., 2009), these priors have gained popularity in various contexts, including dynamic shrinkage models (Kowal et al., 2019), graphical models (Li et al., 2019b), and Bayesian neural network compression (Louizos et al., 2017). The class of global-local shrinkage priors includes a wide variety of formulations (Tipping, 2001; Johnstone and Silverman, 2004; Griffin and Brown, 2005; Park and Casella, 2008; Bhadra et al., 2019a). Among these, the horseshoe prior (Carvalho et al., 2009) has emerged as a particularly attractive choice because of its strong theoretical properties and empirical performance in high-dimensional settings (Datta and Ghosh, 2013; van der Pas et al., 2014, 2017a,b; Bhadra et al., 2019b; Hahn et al., 2020). We focus on the horseshoe prior to introduce continuous shrinkage directly on the tree

step heights. This approach retains all covariates while adaptively shrinking their contributions. The proposed methodology is readily extendable to other global-local shrinkage priors that allow Gibbs sampling and could be further generalised to incorporate different shrinkage strategies with additional computational effort.

Our work contributes to the literature in several ways:

1. We introduce a novel regularisation strategy for Bayesian Additive Regression Trees based on the step-height prior, where we use the horseshoe prior to induce continuous shrinkage rather than relying solely on regularisation via the tree structure.
2. We develop a computational framework for fitting these models via reversible jump Metropolis-Hastings. The implementation is publicly available in the R package `ShrinkageTrees` (Jacobs, 2025).
3. We demonstrate how this framework can be effectively applied to estimate heterogeneous treatment effects in survival data, with a particular focus on high-dimensional covariates.

The remainder of this paper is organised as follows. In Section 2 we describe the causal framework and notation. In Section 3 we introduce the model formulation and prior specification. In Section 4 we describe the computational strategy and posterior inference procedure. We present the simulation results in Section 5. Section 6 provides a detailed case study of pancreatic cancer data. We conclude with a discussion in Section 7.

2 Causal framework

2.1 Modelling of causal effects

Let T denote the non-negative survival time and C denote the censoring time. We observe the follow-up time $Y = \min(T, C)$ along with the censoring indicator $\delta \in \{0, 1\}$, where $\delta = 1$ if the event is observed and $\delta = 0$ if the observation is right-censored. Let $A \in \{0, 1\}$ be a binary treatment indicator, where $A = 1$ corresponds to the treated group and $A = 0$ to the control group. Covariates are denoted by $X \in \mathbb{R}^p$, where p is the number of observed pre-treatment variables. The covariates may include potential confounders. We do not distinguish between various types of covariates in our notation, such as confounders, prognostic factors, moderators, or predictors of treatment assignment (Herren and Hahn, 2020). Throughout, we use capital letters (e.g., T , A , X) to denote random variables, and lowercase letters (e.g., t , a , x) to denote their realisations. We consider a sample of n independent observations.

We assume an accelerated failure time (AFT) model (Buckley and James, 1979) for the potential survival times. The AFT model relates the logarithm of the survival time to a regression function. We decompose the log-transformed outcome into a *prognostic* component and a *treatment effect* component (Hahn et al., 2020):

$$\log T(a) = f(x, \hat{e}(x)) + a \cdot \tau(x) + \varepsilon, \quad (2)$$

where $\varepsilon \sim \mathcal{N}(0, \sigma^2)$ denotes the error term. The function $f(x, \hat{e}(x))$ models the baseline prognosis and incorporates the estimated propensity score $\hat{e}(x)$. The propensity score, $e(x) = \mathbb{P}(A = 1 | X = x)$, is the probability of treatment given covariates (Rosenbaum and Rubin, 1983). The function $\tau(x)$ directly models the treatment effect. In Section 3, we describe a novel regression framework for f and τ that builds on Bayesian regression trees and incorporates a horseshoe prior to handle the high-dimensional covariates. We refer to model (2) with horseshoe prior on the step heights of f and τ as the *Causal Horseshoe Forest*.

The AFT model offers several advantages in the context of causal inference with survival data. The AFT model provides a *collapsible* estimand: the acceleration factor, defined as the ratio of expected survival times under treatment and control, remains invariant when conditioning on additional non-confounding covariates (Robins, 1992; Aalen et al., 2015; Crowther et al., 2023). This implies that $\tau(x)$ can be meaningfully averaged across covariate distributions to obtain the marginal causal effect without introducing bias due to non-collapsibility. Collapsibility is a desirable property in causal inference, as it ensures interpretability and comparability of marginal and conditional effects. In contrast, commonly used hazard-based measures, such as the hazard ratio

in the Cox model, are non-collapsible (Hernán, 2010; Martinussen and Vansteelandt, 2013; Aalen et al., 2015). Furthermore, Hougaard (1999) showed that AFT models are robust to omitted covariates, enhancing their suitability for observational studies.

We include the estimated propensity score in the outcome model to improve causal effect estimation in high-dimensional settings. This inclusion helps to control for confounding and mitigates regularisation-induced confounding, where aggressive shrinkage of confounders can bias treatment effect estimates (Hahn et al., 2020; Ray and van der Vaart, 2020). The propensity score acts as a balancing score: given the propensity score, covariates and treatment assignment become independent (Rosenbaum and Rubin, 1983). We incorporate the *estimated* propensity score directly in the prognostic regression function $f(x, \hat{e}(x))$ to avoid feedback between the outcome and treatment models. Although this approach is not dogmatically Bayesian and does not propagate uncertainty from the propensity score estimation (Zigler et al., 2013), it improves performance in finite samples (Hahn et al., 2020). We estimate the propensity score using a tree-based model specifically designed for high-dimensional covariates and binary treatment assignment.

2.2 Estimands and identification assumptions

We define causal estimands within the potential outcomes framework (Rubin, 1974, 1978; Neyman, 1990). For each individual, let $T(1)$ and $T(0)$ represent the survival times that would be observed under treatment and control, respectively. Likewise, $C(1)$ and $C(0)$ denote the potential censoring times corresponding to each level of treatment. We focus on the conditional average treatment effect (CATE), defined as the difference in expected log survival times under treatment and control, conditional on observed covariates:

$$\text{CATE}(x) := \mathbb{E}[\log T(1) - \log T(0) \mid X = x]. \quad (3)$$

The CATE captures heterogeneity in treatment effects across subgroups defined by covariate profiles $X = x$. Additionally, we consider the average treatment effect (ATE):

$$\text{ATE} := \mathbb{E}[\log T(1) - \log T(0)]. \quad (4)$$

We rely on common assumptions to identify $\tau(x)$ from observational data (Imbens and Rubin, 2015). The first is the *Stable Unit Treatment Value Assumption* (SUTVA), which rules out interference across units and presumes each individual has well-defined potential outcomes under both treatment conditions. This implies that the observed survival time can be expressed as $T = AT(1) + (1 - A)T(0)$. We assume *unconfoundedness* (see (1)) and *positivity*. Positivity requires that for all covariate profiles x each treatment arm has a non-zero probability of assignment:

$$0 < e(x) < 1. \quad (5)$$

Finally, we assume *independent censoring*, meaning that the censoring mechanism is conditionally independent of the survival time given treatment and covariates:

$$C(a) \perp\!\!\!\perp T(a) \mid X = x \quad \text{for } a \in \{0, 1\}. \quad (6)$$

The causal effect is identifiable from the observed data under these assumptions (Imbens, 2004), i.e. $\mathbb{E}[\log T(a) \mid X = x] = \mathbb{E}[\log T \mid X = x, A = a]$ for each $a \in \{0, 1\}$. As a result, the CATE can be expressed in terms of observable quantities as:

$$\text{CATE}(x) = \mathbb{E}[\log T \mid X = x, A = 1] - \mathbb{E}[\log T \mid X = x, A = 0] = \tau(x). \quad (7)$$

The final equality follows from model assumption (2). This identification enables a direct modelling approach of the conditional average treatment effect.

3 Bayesian regression trees

In this section, we describe how we adapt the Bayesian Additive Regression Trees (BART) prior (Chipman et al., 2010) to high-dimensional covariates by introducing a horseshoe prior on the step heights. This approach shifts regularisation from the tree structure (e.g. Linero (2018)) to the step height parameters. We start with an overview of how BART is applied to model log survival times under the accelerated failure time (AFT) framework. We detail our novel adaptation using a global-local shrinkage prior. We then explain how the model accommodates censored outcomes. Finally, we discuss default hyperparameter choices.

3.1 Overview of Bayesian Additive Regression Trees (BART)

We adapt the BART model to estimate the conditional mean function $\mathbb{E}[\log T_i \mid X_i = x]$ in the AFT model. The uncensored survival times are modelled as a noisy sum of trees:

$$\log T_i = \sum_{j=1}^m g(X_i; \mathcal{T}_j, \mathcal{H}_j) + \varepsilon_i, \quad \varepsilon_i \sim \mathcal{N}(0, \sigma^2), \quad (8)$$

where each \mathcal{T}_j is a binary decision tree that defines recursive partitioning rules over the covariate space, and $\mathcal{H}_j = \{h_{j1}, \dots, h_{jL_j}\}$ denotes the set of step height associated with the L_j leaves of tree \mathcal{T}_j . We extend this model to accommodate censored survival times in Section 3.4.

For a given input x , the function $g(x; \mathcal{T}_j, \mathcal{H}_j)$ maps x to a leaf node ℓ in \mathcal{T}_j and returns the corresponding value $h_{j\ell}$. Each tree partitions the covariate space into disjoint regions, assigning a constant prediction to each region (see Figure 1). The prediction of the j -th tree for individual i is obtained by:

$$g(X_i; \mathcal{T}_j, \mathcal{H}_j) = \sum_{\ell=1}^{L_j} h_{j\ell} \cdot \mathbb{1}(X_i; \mathcal{T}_j, \ell), \quad (9)$$

where $\mathbb{1}(X_i; \mathcal{T}_j, \ell) = 1$ if X_i is assigned to leaf ℓ in tree \mathcal{T}_j , and zero otherwise.

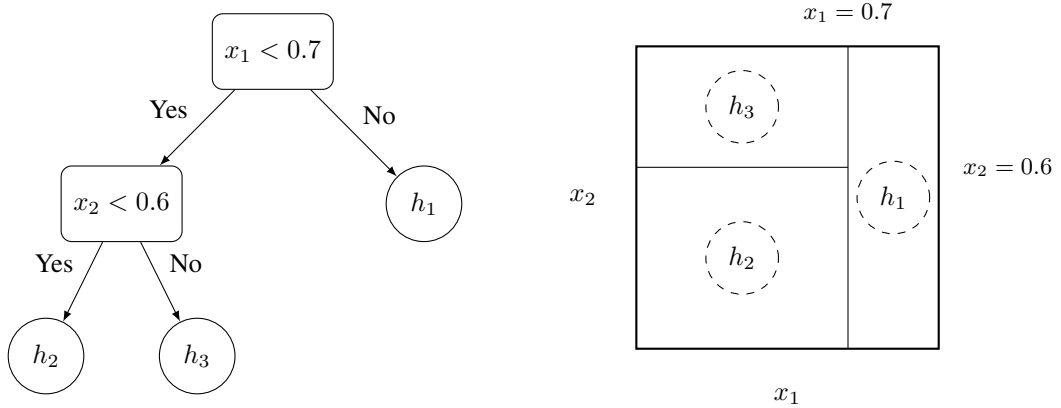


Figure 1: Example of a decision tree with the corresponding partition of the covariate space $[0, 1]^2$ and the associated step-heights $\mathcal{H} = \{h_1, h_2, h_3\}$.

A prior is specified over the ensemble $\{(\mathcal{T}_j, \mathcal{H}_j)\}_{j=1}^m$ by independently assigning a prior on the tree structure and a conditional prior on the step heights given the tree:

$$p(\mathcal{T}_j, \mathcal{H}_j) = p_{\mathcal{T}}(\mathcal{T}_j)p_{\mathcal{H}}(\mathcal{H}_j \mid \mathcal{T}_j) \quad \text{for } j = 1, \dots, m. \quad (10)$$

These define the two key components of the BART prior and are described by Chipman et al. (1998). The prior $p_{\mathcal{T}}(\mathcal{T})$ on the tree structure \mathcal{T} is a heterogeneous Galton-Watson branching process (Ročková and Saha, 2019). The prior $p_{\mathcal{H}}$ on the step heights \mathcal{H} is defined conditionally on the tree structure \mathcal{T} . The step heights $h_{j\ell}$ are assigned a default independent Gaussian priors of the form:

$$h_{j\ell} \sim \mathcal{N}\left(0, \frac{1}{4\sqrt{m}}\right), \quad (11)$$

where the variance is scaled to ensure that the prior places approximately 95% of its mass within the observed range of the response. This prior is conjugate, enabling efficient non-reversible updates using a Gibbs sampler. We modify this prior to accommodate continuous shrinkage of the step height parameters.

3.2 Horseshoe prior on the step heights

We present our novel formulation of step height prior based on a global-local shrinkage prior. Given a tree \mathcal{T} with L leaf nodes, we specify a prior on the set of step heights $\mathcal{H} = \{h_1, h_2, \dots, h_L\}$. To achieve shrinkage in high-dimensional covariate spaces, we use a class of continuous shrinkage priors on the set of step heights. This class can be represented as a scale mixture of normal distributions. In general form, the prior $p_{\mathcal{H}}$ is specified hierarchically:

$$\begin{aligned} h_{\ell} \mid \lambda_{\ell}^2, \tau^2, \omega &\sim \mathcal{N}(0, \omega \lambda_{\ell}^2 \tau^2), \\ \lambda_{\ell}^2 &\sim p(\lambda), \\ \tau^2 &\sim p(\tau), \end{aligned} \quad (12)$$

where $\ell = 1, \dots, L$, and ω is a fixed hyperparameter that ensures appropriate scaling of the prior variance relative to the tree-based model structure.

The horseshoe prior (Carvalho et al., 2009; Polson and Scott, 2011) arises by specifying half-Cauchy distributions for both the global and local shrinkage parameters:

$$\tau \sim \mathcal{C}^+(0, \alpha_{\tau}) \quad \text{and} \quad \lambda_{\ell} \sim \mathcal{C}^+(0, \alpha_{\lambda}) \quad \text{for } \ell = 1, \dots, L, \quad (13)$$

where $\mathcal{C}^+(0, \alpha)$ denotes the half-Cauchy distribution with location zero and scale parameter $\alpha > 0$. Note that the median of the distribution equals α , while the mean and variance do not exist due to the heavy tails. We refer to this specification of the prior as a *Horseshoe Forest*. A Horseshoe Forest refers specifically to a single learner for the outcome, as in (8). In contrast, the *Causal Horseshoe Forest* decomposes the outcome into a prognostic function and a treatment effect function (see (2)), each modelled by its own Horseshoe Forest.

This formulation falls within the class of global-local shrinkage priors (Polson and Scott, 2011). The *global shrinkage parameter* τ governs the overall degree of shrinkage, encouraging all step heights to be small, while the *local shrinkage parameters* λ_{ℓ} allow individual step heights h_{ℓ} to deviate from this global tendency when supported by the data. In the tree-based context, the local shrinkage parameters refer to the values assigned to individual leaf nodes, each associated with a distinct region of the covariate space, whereas the global shrinkage parameter is shared across all leaf nodes. This hierarchical structure enables the model to suppress noise in regions lacking signal while preserving flexibility in regions where effects are present. The horseshoe prior is particularly well-suited for this task, as it can adapt to varying degrees of sparsity without imposing excessive shrinkage on substantial signals (van der Pas et al., 2017a,b; Bhadra et al., 2019b).

The global shrinkage parameter τ can be specified either as a single parameter shared across the entire forest or assigned separately per tree. We adopt the latter approach and assign a separate global shrinkage parameter to each tree. This choice is motivated by two considerations. First, assigning independent global shrinkage parameters preserves the prior independence between trees. This ensures that each tree remains a weak learner and aligns with the original boosting literature. Weak learners have limited individual accuracy and are

combined to form a strong ensemble learner (Schapire, 1990; Freund and Schapire, 1997). Second, each tree partitions the covariate space differently and may focus on distinct regions with varying signal strength. A shrinkage parameter shared across the forest would force the same level of regularisation across the entire covariate space. This would be inefficient in heterogeneous settings. Tree-specific shrinkage allows the model to adapt locally: it can apply more shrinkage in noisy regions and less in informative ones.

We prefer continuous shrinkage over exact sparsity in high-dimensional causal inference. Model selection methods like LASSO-based methods (Belloni et al., 2014; Shortreed and Ertefaie, 2017) or DART (Linero, 2018) induce sparsity by forcing some coefficients to be exactly zero, whereas shrinkage priors such as the horseshoe continuously pull estimates toward zero without fully excluding the respective covariates. This distinction is particularly relevant in causal settings, where omitting covariates risks violating the unconfoundedness assumption (see (1)).

From a conceptual perspective, the use of continuous shrinkage priors in tree-based models is also supported by their connection to the classical normal means problem (James and Stein, 1961). If the covariate space were partitioned into n leaf nodes, each containing a single observation, the model would reduce to a set of independent normals centred at the leaf-specific means. Although such fine partitions are unlikely under the prior, the Bayesian tree ensemble can be viewed as performing Bayesian model averaging over normal means models that cluster observations based on covariate similarity. This connection also supports recent advocacy for Bayesian model averaging in causal inference (Wang et al., 2012; Zigler, 2016; Horii, 2021; Antonelli and Cefalu, 2020). This perspective becomes explicit in Section 4.3, where we describe a full conditional posterior draw of the step height parameters.

3.3 Choice of hyperparameters

We follow the default recommendations of Chipman et al. (2010) regarding the hyperparameters governing the prior on the tree structure. Empirical evaluations suggest that the influence of these parameters is negligible in our setting. We set the number of trees to 200 for both the prognostic and treatment effect forests. This contrasts with the recommendation of Hahn et al. (2020), who advocate using a smaller number of trees for the treatment effect model as a form of regularisation. In our approach, regularisation is instead achieved through the prior on the step heights. We have found that using a larger number of trees, which induces a finer partition of the high-dimensional covariate space, improves estimation in this context.

We adopt an empirical approach to set the prior hyperparameters, following the recommendation of Chipman et al. (2010). Specifically, we centre and standardise the log-transformed survival times using preliminary estimates of the mean and variance, obtained either from a linear AFT model for high-dimensional data (Kumari et al., 2025) or from an intercept-only AFT model. For the Horseshoe Forest model, which uses a single forest, we set the variance scaling parameter to $\omega = 1$. In the Causal Horseshoe Forest model, where the outcome is modelled as the sum of two forests for $f(x)$ and $\tau(x)$, we set $\omega = \frac{1}{2}$ to ensure that sufficient prior mass is allocated across the observed outcome range.

The global and local shrinkage parameters τ and λ are assigned half-Cauchy priors with scale parameters α_τ and α_λ , respectively. For simplicity, we set $\alpha := \alpha_\tau = \alpha_\lambda$. Some studies recommend using a different prior scale for the global parameter τ than for the local parameters λ_ℓ to better control overall shrinkage (Piironen and Vehtari, 2017). In our experiments, we found that setting the same scale for both worked well in practice. This fully Bayesian specification remains adaptive and robust across various settings. We parametrise the scale as $\alpha = \frac{k}{\sqrt{m}}$ for some $k > 0$, where m denotes the number of trees in the respective forest. The choice of k governs the level of shrinkage. We recommend setting $k = 1$ for conservative shrinkage, $k = 0.1$ for moderate shrinkage, and $k = 0.05$ for more aggressive shrinkage. At the start of the chain, a small value for k prevents the sampler from becoming trapped in local regions. As the chain converges toward its stationary distribution, the heavy-tailed nature of the horseshoe prior allows the posterior to explore the full parameter space. In practice, we recommend using $k = 0.1$ as a default or selecting k via cross-validation. We perform cross-validation for censored data using the concordance index (C-statistic) (Harrell et al., 1982), computed on

held-out test predictions.

3.4 Censored and binary outcomes

We account for censoring through data augmentation within the Gibbs sampler (Tanner and Wong, 1987). Censored event times are treated as latent variables and sampled from their full conditional posterior distributions at each iteration. We adopt this strategy in both the Horseshoe Forest and Causal Horseshoe Forest to account for censoring in survival outcomes.

The model also supports binary outcomes. We follow the probit approach of Chipman et al. (2010), which uses a latent Gaussian variable linked to each binary response. This latent variable is modelled as a sum of trees, using the data augmentation scheme of Albert and Chib (1993). We use the same default hyperparameters as in the continuous setting and report supporting simulation results in Supplementary Material S.3. We implement this binary extension only for the Horseshoe Forest and use it to estimate the propensity score.

4 Posterior inference

Posterior inference is performed using a Markov Chain Monte Carlo (MCMC) algorithm. We extend the standard Metropolis-within-Gibbs sampler used in Bayesian additive regression trees to a reversible jump-within-Gibbs scheme (Green, 1995). This extension is required because the global-local horseshoe prior on the step heights breaks the conjugacy used in the original BART algorithm (Chipman et al., 2010). The original independent Gaussian prior (11) allows analytical integration over the step heights. This enables separate updates of the tree structures and step heights. We instead use a reversible jump Metropolis–Hastings step to jointly update both the tree structure and the step heights. Each MCMC iteration alternates between updating the prognostic and treatment effect forests using a Bayesian backfitting strategy (Hastie and Tibshirani, 2000).

In the remainder of this section:

1. **Outer Gibbs sampler.** We describe the Gibbs sampling strategy for updating the components of the decomposed AFT model. Separate forests are specified for the prognostic and treatment effect functions, and survival times are handled using data augmentation.
2. **Reversible jump step.** We detail the reversible jump Metropolis–Hastings step for updating a single tree. Our approach introduces a novel proposal mechanism for the step heights and local shrinkage parameters. These candidate values are drawn from pseudo Gibbs updates informed by the parent node, which improves efficiency and mixing.
3. **Full conditional updates.** We describe the full conditional posterior updates for the step height parameters, conditional on a fixed tree structure. This includes efficient matrix-based sampling and closed-form updates for the global and local shrinkage parameters under the horseshoe prior. We highlight the connection to classical normal means models, which provides intuition for this structure.

4.1 Outer Gibbs sampler

For both the prognostic regression function $f(x)$ and the treatment effect regression function $\tau(x)$, we specify separate Horseshoe Forests. We denote the ensemble for $f(x)$ by $(\mathcal{T}_j^f, \mathcal{H}_j^f)_{j=1}^{m_f}$ and for $\tau(x)$ by $(\mathcal{T}_j^\tau, \mathcal{H}_j^\tau)_{j=1}^{m_\tau}$, where m_f and m_τ represent the number of trees in each respective forest. The outer Gibbs sampler is summarised in Algorithm 1.

The trees in each forest are iteratively updated conditional on all other trees. This conditional updating step depends on the current model state only through the n residuals, which are derived from the model in Equation (2). Specifically, the residuals for the j -th tree in the prognostic forest and treatment effect forest are

given by:

$$\mathcal{R}_j^f := \log T^o - \sum_{J=1, J \neq j}^{m_f} f(X; \mathcal{T}_J^f, \mathcal{H}_J^f) - A \sum_{J=1}^{m_\tau} f(X; \mathcal{T}_J^\tau, \mathcal{H}_J^\tau), \quad (14a)$$

$$\mathcal{R}_j^\tau := \log T^o - \sum_{J=1}^{m_f} f(X; \mathcal{T}_J^f, \mathcal{H}_J^f) - A \sum_{J=1, J \neq j}^{m_\tau} f(X; \mathcal{T}_J^\tau, \mathcal{H}_J^\tau), \quad (14b)$$

where T^o denotes the observed or imputed survival times after data augmentation. We refer to \mathcal{R}_j^f as the *prognostic residuals* and to \mathcal{R}_j^τ as the *treatment effect residuals*.

The censored survival times are augmented within the Gibbs sampler. Specifically, at each iteration, these times are imputed by drawing from their conditional distribution. This conditional distribution is a truncated normal, with the lower bound given by the observed censoring time. The framework can be naturally extended to interval-censored data, in which case the truncated normal is bounded by the corresponding interval limits. The truncated normal distribution is centred at the current model-based prediction \widehat{T} of the survival time, computed using (2), and has variance equal to the current draw of σ^2 . Detailed derivations and further discussion can be found in (Tanner and Wong, 1987).

The error variance σ^2 is sampled from its full conditional distribution. The inverse- χ^2 prior is conjugate. This yields an inverse-gamma update based on the residuals $r_i = \log T_i^o - \log \widehat{T}_i$. Detailed derivations can be found in Gelman et al. (2013, Section 3.2 and 14.2).

We adopt the conventional binary treatment indicator A , coded as 1 for treated individuals and 0 for controls, to clearly communicate our model structure and causal assumptions. However, the proposed model can also accommodate the invariant parametrisation introduced by Hahn et al. (2020), which relies on a data-adaptive treatment coding scheme.

Algorithm 1: Outer Gibbs sampler – $(t + 1)$ -th iteration

Input: Previous $(\mathcal{T}_j^f, \mathcal{H}_j^f)^{(t)}$ for $j = 1, \dots, m$, $(\mathcal{T}_j^\tau, \mathcal{H}_j^\tau)^{(t)}$ for $j = 1, \dots, \tilde{m}$, T_i^o for $i = 1, \dots, n$, $\sigma^{2(t)}$

```

1 for  $j = 1$  to  $m^f$  do
2    $\left|$  Compute prognostic residuals  $\mathcal{R}_j^{f(t)}$  using Equation (14a);
3    $\left|$  Sample  $(\mathcal{T}_j^f, \mathcal{H}_j^f)^{(t+1)}$  from  $(\mathcal{T}_j, \mathcal{H}_j) \mid \mathcal{R}_j^{f(t)}, \sigma^2$ ;
4 for  $j = 1$  to  $m^\tau$  do
5    $\left|$  Compute treatment effect residuals  $\mathcal{R}_j^{\tau(t)}$  using Equation (14b);
6    $\left|$  Sample  $(\mathcal{T}_j^\tau, \mathcal{H}_j^\tau)^{(t+1)}$  from  $(\mathcal{T}_j, \mathcal{H}_j) \mid \mathcal{R}_j^{\tau(t)}, \sigma^2$ ;
7 for  $i = 1$  to  $n$  do
8    $\left|$  if  $\delta_i = 0$  then
9      $\left| \left|$  Compute survival time prediction  $\widehat{T}_i^{(t)}$  using Equation (2);
10     $\left| \left|$  Sample  $T_i^{o(t+1)}$  from  $T_i^o \mid Y_i, \widehat{T}_i^{(t)}, \sigma^{2(t)}$ ;
11    $\left|$  else
12      $\left| \left|$  Set  $T_i^{o(t+1)} = Y_i$ ;
13 Sample  $\sigma^{2(t+1)}$  from  $\sigma^2 \mid \left\{ (\mathcal{T}_j^f, \mathcal{H}_j^f)^{(t+1)} \right\}_{j=1}^{m^f}, \left\{ (\mathcal{T}_j^\tau, \mathcal{H}_j^\tau)^{(t+1)} \right\}_{j=1}^{m^\tau}, \left\{ T_i^{o(t+1)} \right\}_{i=1}^n$ .

```

4.2 Reversible jump step for updating a tree

The tree structure is jointly updated together with its corresponding set of step heights. We propose a new pair $(\mathcal{T}_j, \mathcal{H}_j)$, which is then accepted or rejected using a Metropolis—Hastings step with a reversible jump move (Green, 1995). The conditional posterior distribution of a single tree factorises as:

$$p((\mathcal{T}_j, \mathcal{H}_j) | \mathcal{R}_j, \sigma^2) \propto p(\mathcal{H}_j | \mathcal{T}_j, \mathcal{R}_j, \sigma^2) \times p(\mathcal{T}_j | \mathcal{R}_j, \sigma^2). \quad (15)$$

This factorisation enables a two-step proposal mechanism: first proposing a new tree structure \mathcal{T}_j , then proposing new step heights \mathcal{H}_j conditional on the proposed structure. The overall proposal is evaluated using the reversible jump acceptance probability to ensure detailed balance.

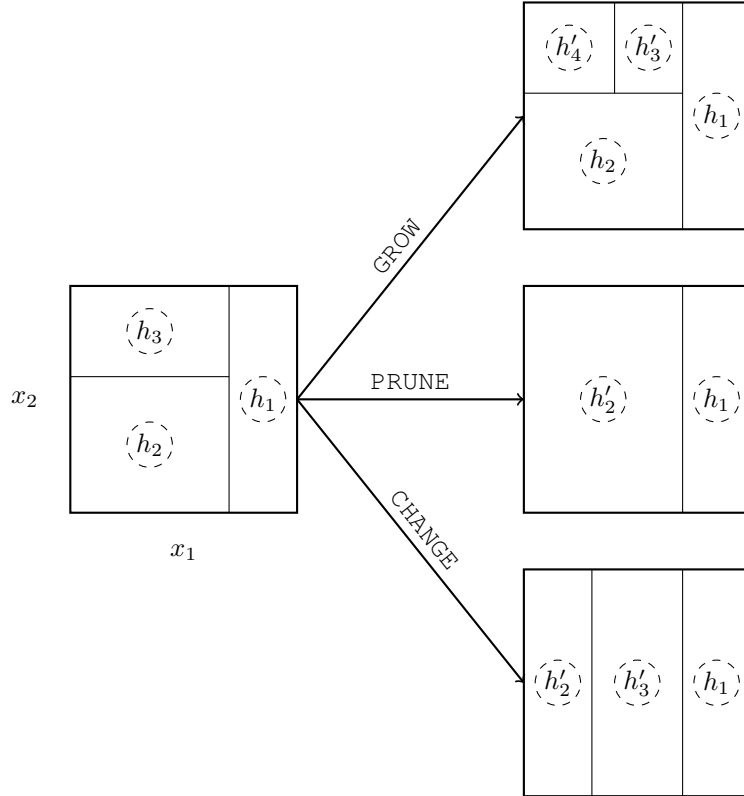


Figure 2: Examples of covariate space partitions induced by each of the three moves on the tree in Figure 1, with corresponding step-heights.

The proposal mechanism relies on three fundamental move types: GROW, PRUNE, and CHANGE (Chipman et al., 1998). Figure 2 schematically illustrates these moves and shows how the dimensionality of the step height parameter vector \mathcal{H}_j changes accordingly. In a GROW move, the tree expands by adding a split, introducing additional step height parameters (and corresponding local horseshoe variance parameters). Conversely, a PRUNE move reduces the tree size by removing a split and eliminating corresponding parameters. A CHANGE move modifies an existing split without altering the number of terminal nodes.

Along with each move, new values for the step height parameters are proposed. The idea is to mimic a Gibbs sampler locally: propose new parameters informed by current values, as if the dimension were fixed. While this pseudo Gibbs proposal does not directly sample from the true posterior, it provides a reasonable approximation. This is corrected using the Metropolis—Hastings acceptance step to leave the posterior invariant.

We illustrate the proposal mechanism for the GROW move. Details for the PRUNE and CHANGE moves are provided in Supplementary Material S.2. Suppose we perform a GROW move on leaf L . Then two new child leaves L and $L + 1$ are grown. We propose new values h'_L , h'_{L+1} , λ'_L , and λ'_{L+1} by drawing from conditional distributions informed by the parent node parameters h_L and λ_L . These conditional distributions can be derived using Bayes' rule. We do not need to propose a global shrinkage parameter τ since this dimensionality is not affected by the tree moves.

The horseshoe prior can be rewritten using an auxiliary variable representation (Makalic and Schmidt, 2016):

$$\begin{aligned} \tau^2 | \xi &\sim \mathcal{IG} \left(\frac{1}{2}, \frac{1}{\xi} \right) & \text{and} & \lambda_\ell^2 | \nu_\ell \sim \mathcal{IG} \left(\frac{1}{2}, \frac{1}{\nu_\ell} \right), \\ \xi &\sim \mathcal{IG} \left(\frac{1}{2}, \frac{1}{\alpha^2} \right) & \nu_\ell &\sim \mathcal{IG} \left(\frac{1}{2}, \frac{1}{\alpha^2} \right), \end{aligned} \quad (16)$$

for $\ell = 1, \dots, L$. This representation allows all conditional distributions to be derived in closed form. For notational simplicity, we write \cdot in the conditioning statement to indicate dependence on all other model parameters and the data. For the new node L , the new parameters are sequentially proposed as:

$$\begin{aligned} \nu'_L | \cdot &\sim \mathcal{IG} \left(1, \frac{1}{\alpha} + \frac{1}{\lambda_L^2} \right), \\ \lambda'_L | \cdot &\sim \mathcal{IG} \left(1, \frac{1}{\nu'_L} + \frac{h_L^2}{2\tau^2\omega} \right), \\ h'_L | \cdot &\sim \mathcal{N} \left(\frac{\bar{\mathcal{R}}'_L}{n'_L + \frac{1}{\tau^2\lambda_L'^2\omega}}, \frac{\sigma^2}{n'_L + \frac{1}{\tau^2\lambda_L'^2\omega}} \right), \end{aligned} \quad (17)$$

where $\bar{\mathcal{R}}'_L$ and n'_L denote the sum and count of residuals mapped to child node L by the proposed tree. The same procedure is applied to propose the parameters for node $L + 1$.

A summary of the single-tree update is given in Algorithm 2. Detailed acceptance ratios and derivations are provided in Supplementary Material S.2. The acceptance probabilities coincide with those of Linero (2024).

Algorithm 2: Update of a single tree via reversible jump step

Input: $(\mathcal{T}_j, \mathcal{H}_j), \mathcal{R}_j, T_i^o$ for $i = 1, \dots, n$, σ^2

- 1 Randomly select and perform one of the moves: GROW, PRUNE, or CHANGE;
- 2 Propose new step height parameters corresponding to the proposed tree structure;
- 3 Compute the reversible jump acceptance ratio;
- 4 Draw $U \sim \mathcal{U}[0, 1]$ and accept or reject the proposed $(\mathcal{T}_j, \mathcal{H}_j)$ accordingly;
- 5 Perform a full Gibbs update of the step height parameters \mathcal{H}_j as described in Section 4.

4.3 Full conditional update of step height parameters

After performing a reversible jump Metropolis—Hastings step that acts locally on a specific terminal node of the tree \mathcal{T}_j , we carry out a full conditional update of the associated step height parameters \mathcal{H}_j . Conditional on the current tree structure, the dimensionality of the parameter space remains fixed, enabling efficient Gibbs sampling updates. Given a tree \mathcal{T} and observed covariates x_1, \dots, x_n , the n observations are partitioned into L step heights. This partition can be encoded by a design matrix $\mathcal{D} \in \mathbb{R}^{n \times L}$, where each row contains exactly one entry of 1 and zeros elsewhere, indicating the assigned step height. Specifically, if observation i belongs to leaf ℓ , then $\mathcal{D}_{i\ell} = 1$. For $\mathcal{D} = I_n$ this reduces to a normal means model. By the valid partitions assumption, each row of \mathcal{D} contains at least one non-zero entry, ensuring no empty leaves.

This structure allows us to reformulate the update as a regression problem in terms of the step heights $h = (h_1, \dots, h_L)$:

$$\mathcal{R} \mid \mathcal{D}, h, \sigma^2 \sim \mathcal{N}(\mathcal{D}h, \sigma^2 I_n), \quad (18)$$

where $\mathcal{R} \in \mathbb{R}^n$ denotes the residuals as defined in (14).

The conditional posterior of $h \in \mathbb{R}^L$ is given by (Lindley and Smith, 1972):

$$h \sim \mathcal{N}_L(\Omega^{-1} \mathcal{D}^\top \mathcal{R}, \Omega^{-1}), \quad \text{where } \Omega = \mathcal{D}^\top \mathcal{D} + [\omega \tau^2 \text{diag}(\lambda_1^2, \dots, \lambda_L^2)]^{-1}. \quad (19)$$

Since $\mathcal{D}^\top \mathcal{D}$ is a diagonal matrix with leaf sizes on its diagonal, let n_ℓ denote the number of observations in leaf ℓ and $\bar{\mathcal{R}}_\ell$ the sum of residuals in leaf ℓ . We can then express the conditional posterior of each h_ℓ as:

$$h_\ell \mid \cdot \sim \mathcal{N}\left(\frac{\bar{\mathcal{R}}_\ell}{n_\ell + \frac{1}{\tau^2 \lambda_\ell^2 \omega}}, \frac{\sigma^2}{n_\ell + \frac{1}{\tau^2 \lambda_\ell^2 \omega}}\right). \quad (20)$$

The conditional posteriors for the shrinkage parameters follow directly from the auxiliary parametrisation of the horseshoe prior, as presented in (16):

$$\begin{aligned} \tau^2 \mid \cdot &\sim \text{IG}\left(\frac{L+1}{2}, \frac{1}{\xi} + \frac{1}{2\omega} \sum_{\ell=1}^L \frac{h_\ell^2}{\lambda_\ell^2}\right) \quad \text{and} \quad \lambda_\ell^2 \mid \cdot \sim \text{IG}\left(1, \frac{1}{\nu_\ell} + \frac{h_\ell^2}{2\tau^2 \omega}\right), \\ \xi \mid \cdot &\sim \text{IG}\left(1, \frac{1}{\alpha^2} + \frac{1}{\tau^2}\right) \quad \nu_\ell \mid \cdot \sim \text{IG}\left(1, \frac{1}{\alpha^2} + \frac{1}{\lambda_\ell^2}\right). \end{aligned} \quad (21)$$

All of these conditional distributions are inverse gamma, and together with the Gaussian update for h , enable efficient Gibbs sampling within each tree. This hierarchical structure facilitates scalable and adaptive updates while maintaining strong shrinkage properties, thus improving mixing and posterior exploration.

5 Simulation studies

We perform simulations to assess the accuracy and robustness of the Causal Horseshoe Forest under varying levels of sparsity, dimensionality, and censoring. These experiments illustrate the empirical performance of our method under both linear and non-linear treatment effect functions.

5.1 Simulation set-up

We consider two Causal Horseshoe Forests: one using the default moderate hyperparameter setting ($k = 0.1$) from Section 3.3, and one tuned via 10-fold cross-validation. The default and cross-validated Causal Horseshoe Forests are compared to the benchmark AFT-BART model proposed by Henderson et al. (2020). The AFT-BART model uses a single BART learner to estimate the conditional average treatment effect. We only implement the semiparametric version of AFT-BART, since it is correctly specified. We sample 5,000 posterior draws after a burn-in of 2,500 iterations. We use 1,000 Monte Carlo replications across all scenarios.

We evaluate each method's ability to estimate the population average treatment effect (ATE) and the conditional average treatment effect (CATE). As evaluation metrics, we use the root mean square error (RMSE), coverage probability, and the average length of the credible intervals. For the CATE, these metrics are averaged over the observations. The mean squared error of the CATE is also referred to as the precision in estimating heterogeneous effects (Hill, 2011).

We generate data for each individual $i = 1, \dots, n$ using the following hierarchical structure:

$$\begin{aligned} X_i &\sim \mathcal{U}[0, 1]^p, \\ A_i &\sim \text{Ber}(e(x_i)), \\ \log T_i &\sim \mathcal{N}(f(x_i) + a_i \tau(x_i), 3), \\ C_i &\sim \text{Exp}(\eta), \\ Y_i &= \min(T_i, C_i), \end{aligned} \tag{22}$$

where $\eta > 0$ is chosen via a Monte Carlo procedure to achieve an average censoring rate of approximately 35% across all scenarios. The propensity score and the prognostic functions are defined as:

$$\begin{aligned} e(x_i) &= \Phi(-0.5 + 0.4x_{i1} - 0.1x_{i3} + 0.3x_{i5}), \\ f(x_i) &= \beta_f^\top x_i, \end{aligned} \tag{23}$$

where the entries of β_f follow a spike-and-slab distribution given by $\beta_f \sim (1 - s)\delta_{0_p} + s\mathcal{N}(0_p, I_p)$, with sparsity $s = 0.1$. We consider two treatment effect functions:

$$\begin{aligned} (\text{Linear}) \quad \tau(x_i) &= 1 + x_{i1} - 2x_{i2} + 3x_{i3} - 4x_{i4} + 5x_{i5} + \beta_\tau^\top x_i, \\ (\text{non-linear}) \quad \tau(x_i) &= 10 \sin(\pi x_{i1} x_{i2}) + 20(x_{i3} - 0.5)^2 + 10x_{i4} + 5x_{i5}, \end{aligned} \tag{24}$$

where the entries of β_τ also follow a spike-and-slab distribution with $s = 0.05$. The linear scenario explicitly introduces confounding while keeping sparsity constant through the $\beta_\tau^\top x$ term. The non-linear scenario follows the benchmark Friedman function (Friedman, 1991). In this scenario the number of contributing covariates is fixed. As p increases, the model effectively becomes sparser. We consider three covariate dimensions $p = 100, 1000, 5000$ and keep the sample size fixed at $n = 200$.

The non-linear scenario is examined in greater depth. We increased the covariate dimension incrementally from low-dimensional $p = 10$ to high-dimensional $p = 1000$ and examined different levels of censoring. We used the same simulation setup and data-generating process as before but reduced the sample size to $n = 100$. We considered three censoring levels: low (ca. 10%), medium (ca. 35%), and high (ca. 60%). The Causal Horseshoe Forest with default hyperparameter settings is compared to the benchmark AFT-BART model.

5.2 Results

The Causal Horseshoe Forest outperforms AFT-BART as the covariate dimension increases. The results are presented in Figure 3 and also summarized in table form in Section S.3 of the Supplementary Material. In the low-dimensional setting $p = 100$, both methods show similar ATE prediction error. The Causal Horseshoe Forest maintains better performance as p grows. The Causal Horseshoe Forest achieves consistently lower CATE prediction error, with the difference becoming more substantial in higher-dimensional settings. Coverage of the ATE remains close to nominal levels in the low-dimensional setting. However, only Causal Horseshoe Forest maintains nominal coverage in higher-dimensional settings. CATE coverage falls slightly below the nominal level but remains stable around 80% with the default setting and 90% with cross-validation across dimensions. The cross-validated version of the Causal Horseshoe Forest shows marginally lower RMSE and higher coverage across settings, but at the cost of wider credible intervals. Overall, the default hyperparameter setting provides a good balance between accuracy and interval width.

In the non-linear scenario, the Causal Horseshoe Forest consistently outperforms AFT-BART across all covariate dimensions and censoring levels. The results are presented in Figure 4. Our method maintains lower RMSE for both the ATE and CATE, with the performance gap widening as the number of covariates increases. This advantage is especially pronounced under high censoring, where AFT-BART shows a sharp increase in error, while the Causal Horseshoe Forest remains stable. The results illustrate the robustness of our approach in challenging high-dimensional and heavily censored settings. In lower-dimensional settings

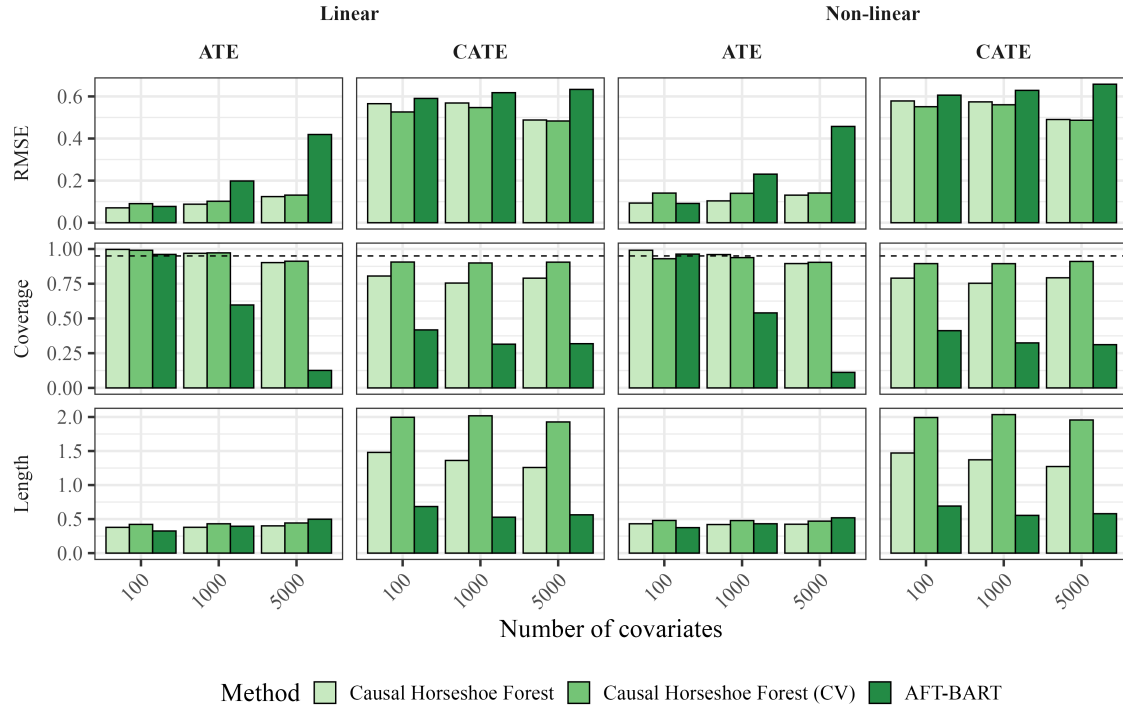


Figure 3: Simulation results for both linear and non-linear scenarios with performance summaries for the CATE and ATE estimation. From top to bottom, the panels display RMSE, empirical coverage (dotted line indicates the nominal 95% level), and average confidence interval length.

$p = 10$, both methods perform similarly, but as p grows, AFT-BART deteriorates quickly, confirming the benefit of shrinkage-based regularisation. These findings confirm our earlier results, demonstrating that the Causal Horseshoe Forest offers stable and accurate treatment effect estimates as dimensionality increases. The method also performs robustly across different levels of censoring.

We provide additional simulation results to further assess the robustness of the proposed methodology in Supplementary Material S.3. These include scenarios with highly correlated covariates, misspecification of the error distribution, and a dense high-dimensional setting. The results broadly support our findings and confirm the stability and competitive performance of the Causal Horseshoe Forest across a range of high-dimensional scenarios.

6 Case study: pancreatic cancer

Pancreatic ductal adenocarcinoma (PDAC) is among the most aggressive and deadly cancers, characterised by rapid progression, late-stage detection, and likely liver metastasis (Pereira and Chio, 2019). The long-term outlook for patients remains poor, with median survival below six months and a five-year survival rate under 5% (Kamisawa et al., 2016; Li et al., 2019a). PDAC exhibits substantial heterogeneity across patients, as highlighted by The Cancer Genome Atlas (TCGA) project (Sidaway, 2017). Unlike many other malignancies, PDAC typically remains asymptomatic until it reaches an advanced stage. Surgical resection is therefore often the only curative option, typically followed by adjuvant radiation therapy.

We study the causal effect of adjuvant radiotherapy on survival while adjusting for genetic and clinical factors

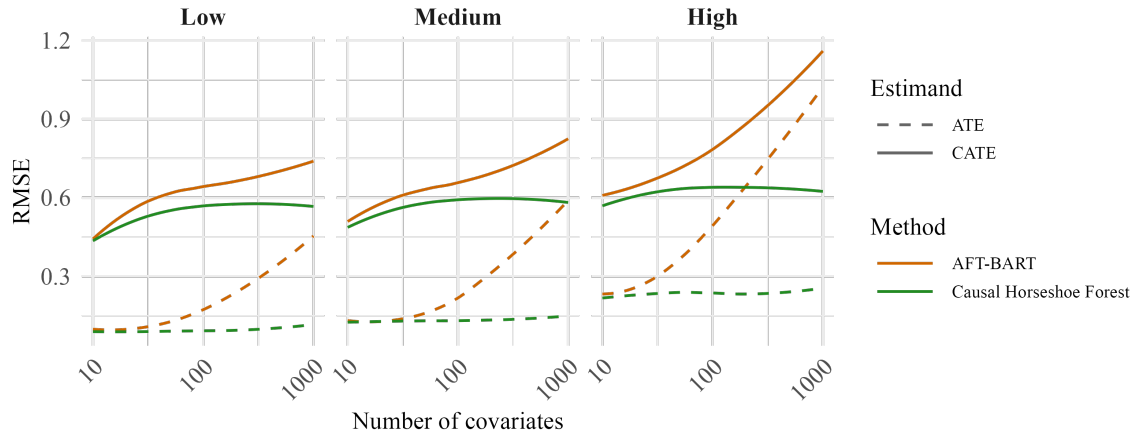


Figure 4: Performance comparison of the Causal Horseshoe Forest and AFT-BART methods across different numbers of covariates p and censoring levels in the Friedman scenario. The plots show the prediction error (RMSE) for both the average treatment effect (ATE) and conditional average treatment effect (CATE). Scenarios correspond to low (10%), medium (35%), and high (60%) levels of censoring.

that may confound or modify this effect. We analyse data from the TCGA-PAAD cohort (Sidaway, 2017). The dataset contains gene expression and clinical information for 181 PDAC tumours. Data is curated via the `pdacR` package (Torre-Healy et al., 2023). We excluded 51 patients with missing values in either survival time, censoring status, or treatment assignment. This leaves 130 patients. The outcome is overall survival, subject to right-censoring. The observed censoring rate is 47%.

The analysis includes several clinical covariates (see Supplementary Material S.5) and gene expression profiles. A number of well-established genetic alterations drive PDAC tumorigenesis (Stefanoudakis et al., 2024). We *a priori* include a subset of genes previously linked to PDAC in the literature (see Supplementary Material S.5). Additionally, we incorporate the 3,000 genes with the highest median absolute deviation (MAD) across patients to capture the most variable and remove low-variability genes. This approach emphasises genes with substantial variation, which are more likely to carry informative signal for downstream modelling and reduces noise from uninformative or uniformly expressed genes (Hackstadt and Hess, 2009; Zhang et al., 2018).

Median follow-up time is 23.3 months. This is computed using the reverse Kaplan-Meier method (Schemper and Smith, 1996). The estimated 2-year overall survival probability is 39.2%. Figure 5 shows Kaplan-Meier survival curves stratified by treatment arm.

We fit a Causal Horseshoe Forest to the data with aggressive default settings in Section 3.3. We performed stratified 10×5 -fold cross-validation to validate the choice of hyperparameter k . Cross-validation showed no difference in terms of predictive performance across different choice of k (see Supplementary Material S.5). We assessed convergence using trace plots of σ^2 (see Supplementary Material S.5). After a burn-in of 5,000 iterations, we retained 5,000 posterior samples for inference. The fitted model achieved a concordance index of 0.80, indicating good performance.

Figure 6 shows the posterior distribution of the average treatment effect (ATE), with the 95% credible interval marked by vertical dashed lines. The posterior mean ATE is approximately 0.75, with a 95% credible interval ranging from 0.40 to 1.11. This distribution is concentrated above zero, providing strong evidence for a positive average treatment effect. These results suggest that adjuvant radiation therapy improves overall survival on average in PDAC patients.

Figure 7 shows the posterior CATEs for each individual. Each horizontal line represents a 95% credible

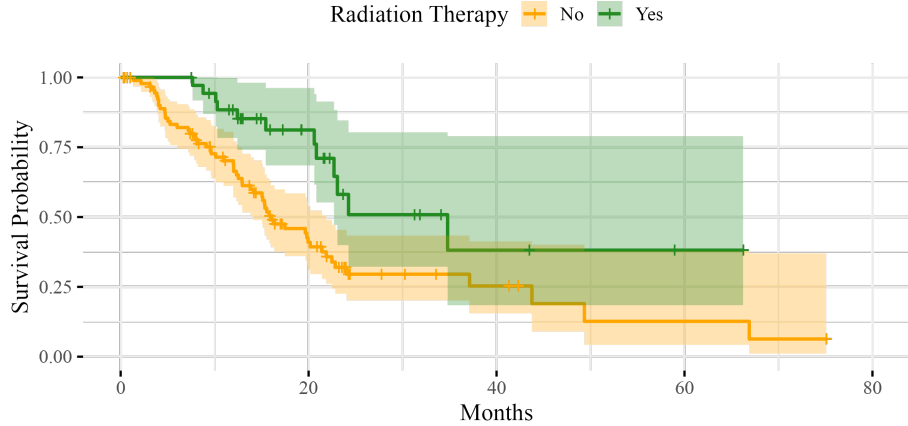


Figure 5: Kaplan–Meier survival curves for each treatment arm in the PDAC dataset.

interval for the conditional average treatment effect. Most intervals are wide and include zero. This reflects substantial uncertainty and limited evidence for strong individualised effects. A small subset of patients has intervals entirely above zero. This suggests evidence—if any—for a positive treatment effect. The wide intervals for many patients likely reflect insufficient information to confidently distinguish their individualised treatment effects for individuals with similar characteristics. Nevertheless, the consistent rightward shift of the posterior means supports an overall beneficial and homogeneous effect of the treatment.

The stable treatment assumption is not fully met, as adjuvant radiation therapy is not standardised across patients. Treatment regimens may vary in composition, dosage, and duration. As a result, our analysis estimates the effect of receiving any form of radiation therapy, rather than a single, uniform intervention.

The high mortality rate of pancreatic cancer introduces bias. Some patients may die before becoming eligible for or completing adjuvant radiation therapy. Thus, patients in the treatment group must have survived long enough to initiate and complete therapy. This creates immortal time (Lévesque et al., 2010), a period during which the event cannot occur by definition, potentially biasing results in favour of the treatment group. We provide a preliminary landmark analysis (Anderson et al., 1983; Putter, 2013) in Supplementary Material S.6. A more thorough analysis would require detailed data on treatment timing, which are not available in this study. Future studies with detailed treatment timing data could help to address this bias.

7 Discussion

This work introduces a novel regularisation strategy for Bayesian regression tree ensembles by applying shrinkage directly to the step heights via the horseshoe prior. We use continuous global–local shrinkage to adaptively control model complexity in high-dimensional settings, while retaining all covariates in the model. This provides an alternative to methods that exclude covariates from the model and risk omitting important confounders. Our method captures complex non-linear effects and higher-order interactions in both the prognostic and treatment effect functions. These are essential for modelling heterogeneous treatment responses in survival data.

The estimands considered in this paper focus on average increases in log survival time, both at the population level and conditional on covariate characteristics. While these estimands are widely used in the causal inference literature, they are less common in survival analysis because they require stronger assumptions on the tails of the survival distribution and long-term event dynamics. These assumptions are particularly relevant in settings with long-term survivors, or when survival is affected by immortal time bias. Alternative estimands such

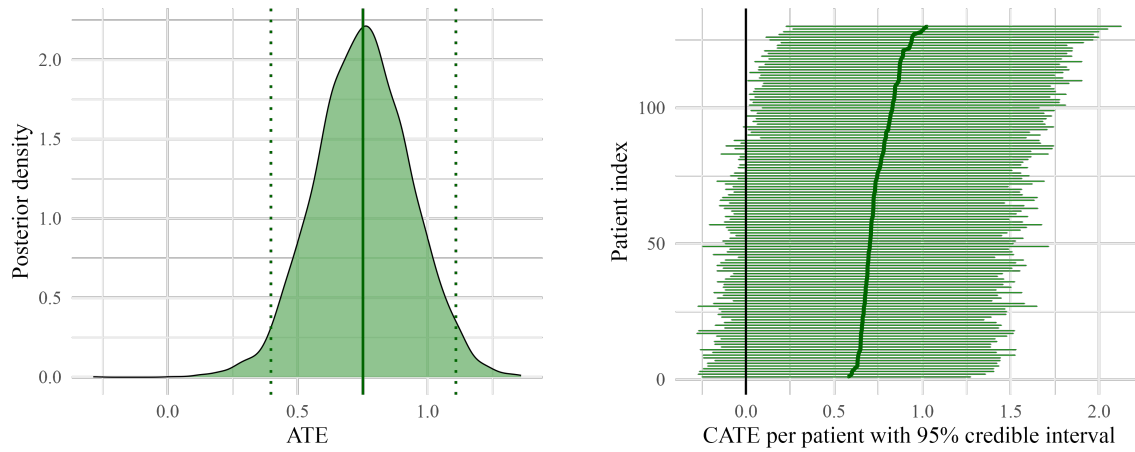


Figure 6: Posterior distribution of the average treatment effect (ATE) of adjuvant chemotherapy on overall survival in PDAC.

Figure 7: Posterior means and 95% credible intervals for the individual CATEs under adjuvant chemotherapy in patients with PDAC.

as the restricted mean survival time (RMST), risk differences or dynamic prediction-based quantities may provide more interpretable or robust summaries of treatment effect. A natural next step is to extend the current framework with cure models or time-dependent structures to target these alternative estimands.

Acknowledgement

The software implementation is available on CRAN: <https://cran.r-project.org/package=ShrinkageTrees>. All data and replication code can be found at: <https://github.com/tijn-jacobs/ShrinkageTrees>.

Funding

Tijn Jacobs and Stéphanie van der Pas were funded by the European Union. Views and opinions expressed are however those of the author(s) only and do not necessarily reflect those of the European Union or the European Research Council Executive Agency. Neither the European Union nor the granting authority can be held responsible for them. This work is supported by ERC grant BayCause, nr. 101074802.

References

O. O. Aalen, R. J. Cook, and K. Røysland. Does Cox analysis of a randomized survival study yield a causal treatment effect? *Lifetime Data Analysis*, 21(4):579–593, 2015. doi: 10.1007/s10985-015-9335-y.

A. Alaa and M. van der Schaar. Limits of estimating heterogeneous treatment effects: Guidelines for practical algorithm design. In J. Dy and A. Krause, editors, *Proceedings of the 35th International Conference on Machine Learning*, volume 80 of *Proceedings of Machine Learning Research*, pages 129–138. PMLR, 2018.

J. H. Albert and S. Chib. Bayesian analysis of binary and polychotomous response data. *Journal of the American Statistical Association*, 88(422):669–679, 1993. doi: 10.2307/2290350.

J. R. Anderson, K. C. Cain, and R. D. Gelber. Analysis of survival by tumor response. *Journal of Clinical Oncology*, 1(11):710–719, 1983.

J. Antonelli and M. Cefalu. Averaging causal estimators in high dimensions. *Journal of Causal Inference*, 8(1):92–107, 2020. doi: 10.1515/jci-2019-0031.

J. Antonelli, M. Cefalu, N. Palmer, and D. Agniel. Doubly robust matching estimators for high dimensional confounding adjustment. *Biometrics*, 74(4):1171–1179, 2018. doi: 10.1111/biom.12883.

J. Antonelli, G. Papadogeorgou, and F. Dominici. Causal inference in high dimensions: A marriage between Bayesian modeling and good frequentist properties. *Biometrics*, 78(1):100–114, 2022. doi: 10.1111/biom.13417.

S. Athey and G. Imbens. Recursive partitioning for heterogeneous causal effects. *Proceedings of the National Academy of Sciences of the United States of America*, 113(27):7353–7360, 2016. doi: 10.1073/pnas.1510489113.

A. Belloni, V. Chernozhukov, and C. Hansen. Inference on treatment effects after selection among high-dimensional controls. *The Review of Economic Studies*, 81(2):608–650, 2014. doi: 10.1093/restud/rdt044.

A. Bhadra, J. Datta, N. G. Polson, and B. Willard. The horseshoe+ estimator of ultra-sparse signals. *Bayesian Analysis*, 14(4):1105–1131, 2019a. doi: 10.1214/18-BA1135.

A. Bhadra, J. Datta, N. G. Polson, and B. Willard. Lasso meets horseshoe: A survey. *Statistical Science*, 34(3):405–427, 2019b. doi: 10.1214/19-STS700.

V. Bonato, V. Baladandayuthapani, B. M. Broom, E. P. Sulman, K. D. Aldape, and K.-A. Do. Bayesian ensemble methods for survival prediction in gene expression data. *Bioinformatics*, 27(3):359–367, 2011. doi: 10.1093/bioinformatics/btq660.

J. Buckley and I. James. Linear regression with censored data. *Biometrika*, 66(3):429–436, 1979. doi: 10.1093/biomet/66.3.429.

A. Caron, G. Baio, and I. Manolopoulou. Estimating individual treatment effects using non-parametric regression models: a review. *Journal of the Royal Statistical Society Series A: Statistics in Society*, 185(3):1115–1149, 2022a. doi: 10.1111/rssa.12824.

A. Caron, G. Baio, and I. Manolopoulou. Shrinkage Bayesian causal forests for heterogeneous treatment effects estimation. *Journal of Computational and Graphical Statistics*, 31(4):1202–1214, 2022b. doi: 10.1080/10618600.2022.2067549.

C. M. Carvalho, N. G. Polson, and J. G. Scott. Handling sparsity via the horseshoe. In D. van Dyk and M. Welling, editors, *Proceedings of the 12th International Conference on Artificial Intelligence and Statistics*, volume 5, pages 73–80. PMLR, 2009.

V. Chernozhukov, C. Cinelli, W. Newey, A. Sharma, and V. Syrgkanis. Long story short: Omitted variable bias in causal machine learning. Working Paper 30302, National Bureau of Economic Research, July 2022. URL <http://www.nber.org/papers/w30302>.

H. A. Chipman, E. I. George, and R. E. McCulloch. Bayesian CART model search. *Journal of the American Statistical Association*, 93(443):935–948, 1998. doi: 10.2307/2670071.

H. A. Chipman, E. I. George, and R. E. McCulloch. BART: Bayesian additive regression trees. *Annals of Applied Statistics*, 4(1):266–298, 2010. doi: 10.1214/09-AOAS285.

M. J. Crowther, P. Royston, and M. Clements. A flexible parametric accelerated failure time model and the extension to time-dependent acceleration factors. *Biostatistics*, 24(3):811–831, 2023. doi: 10.1093/biostatistics/kxac009.

Y. Cui, M. R. Kosorok, E. Sverdrup, S. Wager, and R. Zhu. Estimating heterogeneous treatment effects with right-censored data via causal survival forests. *Journal of the Royal Statistical Society: Series B (Statistical Methodology)*, 85(2):179–211, 2023. doi: 10.1093/rssb/qkac001.

J. Datta and J. K. Ghosh. Asymptotic properties of Bayes risk for the horseshoe prior. *Bayesian Analysis*, 8(1):111–132, 2013. doi: 10.1214/13-BA803.

V. Dorie, J. Hill, U. Shalit, M. Scott, and D. Cervone. Automated versus do-it-yourself methods for causal inference: Lessons learned from a data analysis competition. *Statistical Science*, 34(1):43–68, 2019. doi: 10.1214/18-STS667.

Q. Fan, Y.-C. Hsu, R. P. Lieli, and Y. Zhang. Estimation of conditional average treatment effects with high-dimensional data. *Journal of Business & Economic Statistics*, 40(1):313–327, 2022. doi: 10.1080/07350015.2020.1780879.

M. H. Farrell. Robust inference on average treatment effects with possibly more covariates than observations. *Journal of Econometrics*, 189(1):1–23, 2015. doi: 10.1016/j.jeconom.2015.06.003.

Y. Freund and R. E. Schapire. A decision-theoretic generalization of on-line learning and an application to Boosting. *Journal of Computer and System Sciences*, 55(1):119–139, 1997.

J. H. Friedman. Multivariate adaptive regression splines. *Annals of Statistics*, 19(1):1–67, 1991. doi: 10.1214/aos/1176347963.

A. Gelman, J. B. Carlin, H. S. Stern, D. B. Dunson, A. Vehtari, and D. B. Rubin. *Bayesian Data Analysis*. Chapman & Hall/CRC, 3 edition, 2013. doi: 10.1201/b16018.

P. J. Green. Reversible jump MCMC computation and Bayesian model determination. *Biometrika*, 82(4):711–732, 1995. doi: 10.1093/biomet/82.4.711.

J. E. Griffin and P. J. Brown. Alternative prior distributions for variable selection with very many more variables than observations. *Bayesian Analysis*, 1(2):385–402, 2005. doi: 10.1214/05-BA122.

A. J. Hackstadt and A. M. Hess. Filtering for increased power for microarray data analysis. *Statistics in Medicine*, 28(24):3899–3914, 2009. doi: 10.1002/sim.3727.

P. R. Hahn, J. S. Murray, and C. M. Carvalho. Bayesian regression tree models for causal inference: Regularization, confounding, and heterogeneous effects. *Bayesian Analysis*, 15(3):965–1056, 2020. doi: 10.1214/20-BA1210.

F. E. Harrell, R. M. Calif, D. B. Pryor, K. L. Lee, and R. A. Rosati. Evaluating the yield of medical tests. *JAMA*, 247(18):2543–2546, 1982. doi: 10.1001/jama.1982.03320430047030.

T. Hastie and R. Tibshirani. Bayesian backfitting (with comments and a rejoinder by the authors). *Statistical Science*, 15(3):196–223, 2000. doi: 10.1214/ss/1009212753.

N. C. Henderson, T. A. Louis, G. L. Rosner, and R. Varadhan. Individualized treatment effects with censored data via fully nonparametric Bayesian accelerated failure time models. *Biostatistics*, 21(1):50–68, 2020. doi: 10.1093/biostatistics/kxy028.

M. A. Hernán. The hazards of hazard ratios. *Epidemiology*, 21(1):13–15, 2010. doi: 10.1097/EDE.0b013e3181c1ea43.

R. Herren and P. R. Hahn. A fast and flexible approach for causal inference with high-dimensional covariates. *Statistics and Computing*, 30:991–1007, 2020. doi: 10.1007/s11222-020-09949-4.

J. L. Hill. Bayesian nonparametric modeling for causal inference. *Journal of Computational and Graphical Statistics*, 20(1):217–240, 2011. doi: 10.1198/jcgs.2010.08162.

S. Horii. Bayesian model averaging for causality estimation and its approximation based on gaussian scale mixture distributions. In A. Banerjee and K. Fukumizu, editors, *Proceedings of the 24th International Conference on Artificial Intelligence and Statistics*, volume 130 of *Proceedings of Machine Learning Research*, pages 955–963. PMLR, 2021.

P. Hougaard. Fundamentals of survival data. *Biometrics*, 55:13–22, 1999. doi: 10.1111/j.0006-341X.1999.00013.x.

L. Hu, J. Ji, and F. Li. Estimating heterogeneous survival treatment effect in observational data using machine learning. *Statistics in Medicine*, 40(21):4691–4713, 2021. doi: 10.1002/sim.9090.

L. Hu, J. Ji, R. D. Ennis, and J. W. Hogan. A flexible approach for causal inference with multiple treatments and clustered survival outcomes. *Statistics in Medicine*, 42(5):745–761, 2023. doi: 10.1002/sim.9548.

G. W. Imbens. Nonparametric estimation of average treatment effects under exogeneity: A review. *The Review of Economics and Statistics*, 86(1):4–29, 2004. doi: 10.1162/003465304323023651.

G. W. Imbens and D. B. Rubin. *Causal Inference for Statistics, Social, and Biomedical Sciences: An Introduction*. Cambridge University Press, 2015. doi: 10.1017/CBO9781139025751.

T. Jacobs. *ShrinkageTrees: Regression Trees with Shrinkage Priors*, 2025. URL <https://cran.r-project.org/package=ShrinkageTrees>. R package version 1.0.0.

W. D. James and C. Stein. Estimation with quadratic loss. *Proceedings of the Fourth Berkeley Symposium on Mathematical Statistics and Probability*, 1:361–379, 1961.

I. M. Johnstone and B. W. Silverman. Needles and straw in a haystack: Empirical Bayes estimates of possibly sparse sequences. *Annals of Statistics*, 32(4):1594–1649, 2004. doi: 10.1214/009053604000000030.

T. Kamisawa, L. D. Wood, T. Itoi, and K. Takaori. Pancreatic cancer. *The Lancet*, 388(10039):73–85, 2016. doi: 10.1016/S0140-6736(16)00141-0.

A. Kapelner and J. Bleich. bartmachine: Machine learning with Bayesian additive regression trees. *Journal of Statistical Software*, 70(4):1–40, 2016. doi: 10.18637/jss.v070.i04.

D. R. Kowal, D. S. Matteson, and D. Ruppert. Dynamic shrinkage processes. *Journal of the Royal Statistical Society: Series B (Statistical Methodology)*, 81(4):781–804, 2019. doi: 10.1111/rssb.12325.

P. Kumari, A. Bhattacharjee, G. K. Vishwakarma, and F. Tank. Afthd: Bayesian accelerated failure time model for high-dimensional time-to-event data. *Japanese Journal of Statistics and Data Science*, 2025. doi: 10.1007/s42081-025-00301-5.

L. E. Lévesque, J. A. Hanley, A. Kezouh, and S. Suissa. Problem of immortal time bias in cohort studies: example using statins for preventing progression of diabetes. *BMJ*, 340:b5087, 2010. doi: 10.1136/bmj.b5087.

S. Li, H.-X. Xu, C.-T. Wu, W.-Q. Wang, W. Jin, H.-L. Gao, H. Li, S.-R. Zhang, J.-Z. Xu, Z.-H. Qi, Q.-X. Ni, X.-J. Yu, and L. Liu. Angiogenesis in pancreatic cancer: current research status and clinical implications. *Angiogenesis*, 22(1):15–36, 2019a. doi: 10.1007/s10456-018-9645-2.

Y. Li, B. A. Craig, and A. Bhadra. The graphical horseshoe estimator for inverse covariance matrices. *Journal of Computational and Graphical Statistics*, 28(3):747–757, 2019b. doi: 10.1080/10618600.2019.1575744.

D. V. Lindley and A. F. M. Smith. Bayes estimates for the linear model. *Journal of the Royal Statistical Society. Series B (Methodological)*, 34(1):1–41, 1972.

A. R. Linero. Bayesian regression trees for high-dimensional prediction and variable selection. *Journal of the American Statistical Association*, 113(522):626–636, 2018. doi: 10.1080/01621459.2016.1264957.

A. R. Linero. Generalized Bayesian additive regression trees models: Beyond conditional conjugacy. *Journal of the American Statistical Association*, 120(549):356—369, 2024. doi: 10.1080/01621459.2024.2337156.

Y. Liu, V. Ročková, and Y. Wang. Variable selection with abc bayesian forests. *Journal of the Royal Statistical Society Series B: Statistical Methodology*, 83(3):453–481, 2021. doi: 10.1111/rssb.12423.

C. Louizos, K. Ullrich, and M. Welling. Bayesian compression for deep learning. In *Advances in Neural Information Processing Systems*, volume 30, pages 3288–3298. Curran Associates, Inc., 2017.

E. Makalic and D. F. Schmidt. A simple sampler for the horseshoe estimator. *IEEE Signal Processing Letters*, 23(1):179–182, 2016. doi: 10.1109/LSP.2015.2503725.

T. Martinussen and S. Vansteelandt. On collapsibility and confounding bias in cox and aalen regression models. *Lifetime Data Analysis*, 19(3):279–296, 2013. doi: 10.1007/s10985-013-9256-6.

T. J. Mitchell and J. J. Beauchamp. Bayesian variable selection in linear regression. *Journal of the American Statistical Association*, 83(404):1023–1032, 1988.

J. Neyman. On the application of probability theory to agricultural experiments. essay on principles. section 9. *Statistical Science*, 5(4):465–472, 1990. doi: 10.1214/ss/1177012031. Translated and edited by D.M. Dabrowska and T.P. Speed.

Y. Ning, P. Sida, and K. Imai. Robust estimation of causal effects via a high-dimensional covariate balancing propensity score. *Biometrika*, 107(3):533–554, 2020. doi: 10.1093/biomet/asaa018.

T. Park and G. Casella. The Bayesian lasso. *Journal of the American Statistical Association*, 103(482):681–686, 2008. doi: 10.1198/016214508000000337.

M. A. Pereira and I. I. C. Chio. Metastasis in pancreatic ductal adenocarcinoma: current standing and methodologies. *Genes*, 11(1):6, 2019. doi: 10.3390/genes11010006.

J. Piironen and A. Vehtari. On the hyperprior choice for the global shrinkage parameter in the horseshoe prior. In A. Singh and J. Zhu, editors, *Proceedings of the 20th International Conference on Artificial Intelligence and Statistics*, volume 54 of *Proceedings of Machine Learning Research*, pages 905–913. PMLR, 2017.

N. G. Polson and J. G. Scott. Shrink globally, act locally: Sparse Bayesian regularization and prediction. In J. M. Bernardo, M. J. Bayarri, J. O. Berger, A. F. M. Smith, D. B. Goldstein, and A. P. Dawid, editors, *Bayesian Statistics 9*, pages 501–538. Oxford University Press, 2011. doi: 10.1093/acprof:oso/9780199694587.003.0017.

S. Powers, J. Qian, K. Jung, A. Schuler, N. H. Shah, T. Hastie, and R. Tibshirani. Some methods for heterogeneous treatment effect estimation in high dimensions. *Statistics in Medicine*, 37(11):1767–1787, 2018. doi: 10.1002/sim.7623.

H. Putter. Landmarking. In J. P. Klein, H. C. van Houwelingen, J. G. Ibrahim, and A. A. Tsiatis, editors, *Handbook of Survival Analysis*, chapter 21, pages 441–456. Chapman & Hall/CRC, Boca Raton, 2013.

K. Ray and A. W. van der Vaart. Semiparametric Bayesian causal inference. *Annals of Statistics*, 48(5):2999–3020, 2020. doi: 10.1214/19-AOS1919.

J. M. Robins. Estimation of the time-dependent accelerated failure time model in the presence of confounding factors. *Biometrika*, 79(2):321–334, 1992.

P. R. Rosenbaum and D. B. Rubin. The central role of the propensity score in observational studies for causal effects. *Biometrika*, 70(1):41–55, 1983. doi: 10.2307/2335942.

V. Ročková and E. Saha. On theory for BART. In K. Chaudhuri and M. Sugiyama, editors, *Proceedings of the Twenty-Second International Conference on Artificial Intelligence and Statistics*, volume 89 of *Proceedings of Machine Learning Research*, pages 2839–2848. PMLR, 2019.

D. B. Rubin. Estimating causal effects of treatments in randomized and nonrandomized studies. *Journal of Educational Psychology*, 66(5):688–701, 1974. doi: 10.1037/h0037350.

D. B. Rubin. Bayesian inference for causal effects: The role of randomization. *Annals of Statistics*, 6(1):34–58, 1978. doi: 10.1214/aos/1176344064.

R. E. Schapire. The strength of weak learnability. *Machine Learning*, 5(2):197–227, 1990.

M. Schemper and T. L. Smith. A note on quantifying follow-up in studies of failure time. *Controlled Clinical Trials*, 17(4):343–346, 1996. doi: 10.1016/0197-2456(96)00075-X.

H. Shin and J. Antonelli. Improved inference for doubly robust estimators of heterogeneous treatment effects. *Biometrics*, 2023. doi: 10.1111/biom.13837.

S. M. Shortreed and A. Ertefaie. Outcome-adaptive lasso: Variable selection for causal inference. *Biometrics*, 73(4):1111–1122, 2017. doi: 10.1111/biom.12679.

P. Sidaway. TCGA data reveal a highly heterogeneous disease. *Nature Reviews Clinical Oncology*, 14:648, 2017. doi: 10.1038/nrclinonc.2017.139.

D. Stefanoudakis, M. Frountzas, D. Schizas, N. V. Michalopoulos, A. Drakaki, and K. G. Toutouzas. Significance of tp53, cdkn2a, smad4 and kras in pancreatic cancer. *Current Issues in Molecular Biology*, 46(4):2827–2844, 2024. doi: 10.3390/cimb46040177.

R. Sun and X. Song. A tree-based Bayesian accelerated failure time cure model for estimating heterogeneous treatment effect. *Bayesian Analysis*, 20(2):345–373, 2025. doi: 10.1214/23-BA1402.

M. A. Tanner and W. H. Wong. The calculation of posterior distributions by data augmentation. *Journal of the American Statistical Association*, 82(398):528–540, 1987. doi: 10.2307/2289457.

D. R. Thal and M. M. Finucane. Causal methods madness: Lessons learned from the 2022 acic competition to estimate health policy impacts. *Observational Studies*, 9(3):3–27, 2023. doi: 10.1353/obs.2023.0023.

M. E. Tipping. Sparse Bayesian learning and the relevance vector machine. *Journal of Machine Learning Research*, 1:211–244, 2001. doi: 10.1162/15324430152748236.

L. A. Torre-Healy, R. R. Kawalerski, K. Oh, L. Chrastecka, X. L. Peng, A. J. Aguirre, N. U. Rashid, J. J. Yeh, and R. A. Moffitt. Open-source curation of a pancreatic ductal adenocarcinoma gene expression analysis platform (pdacr) supports a two-subtype model. *Communications Biology*, 6:163, 2023. doi: 10.1038/s42003-023-04461-6.

S. L. van der Pas, B. J. K. Kleijn, and A. W. van der Vaart. The horseshoe estimator: Posterior concentration around nearly black vectors. *Electronic Journal of Statistics*, 8(2):2585–2618, 2014. doi: 10.1214/14-EJS962.

S. L. van der Pas, B. Szabó, and A. W. van der Vaart. Uncertainty quantification for the horseshoe. *Bayesian Analysis*, 12(4):1221–1274, 2017a. doi: 10.1214/17-BA1075.

S. L. van der Pas, B. Szabó, and A. W. van der Vaart. Adaptive posterior contraction rates for the horseshoe. *Electronic Journal of Statistics*, 11(2):3196–3225, 2017b. doi: 10.1214/17-EJS1316.

H. C. van Houwelingen and H. Putter. Dynamic prediction in clinical survival analysis. *CRC Press*, 2011.

S. Wager and S. Athey. Estimation and inference of heterogeneous treatment effects using random forests. *Journal of the American Statistical Association*, 113(523):1228–1242, 2018. doi: 10.1080/01621459.2017.1319839.

C.-H. Wang, G. Parmigiani, and F. Dominici. Bayesian effect estimation accounting for adjustment uncertainty. *Biometrics*, 68(3):661–671, 2012. doi: 10.1111/j.1541-0420.2011.01731.x.

J. Zhang, J. Yang, Y. Zhang, and M. Dong. Transcriptomic analysis reveals molecular subtypes of pancreatic cancer. *BMC Cancer*, 18:769, 2018. doi: 10.1186/s12885-018-4634-x.

C. M. Zigler. The central role of Bayes’ theorem for joint estimation of causal effects and propensity scores. *The American Statistician*, 70(1):47–54, 2016. doi: 10.1080/00031305.2015.1111260.

C. M. Zigler, K. Watts, R. W. Yeh, Y. Wang, B. A. Coull, and F. Dominici. Model feedback in Bayesian propensity score estimation. *Biometrics*, 69(2):263–273, 2013. doi: 10.1111/j.1541-0420.2012.01830.x.

Supplementary Material

S.1 Extra details to the outer Gibbs sampler

This section provides additional technical details on the outer Gibbs sampler described in Section 4.1. A summary of the full sampling scheme is given in Algorithm 1. We elaborate on two key components: (i) the update of the error variance σ^2 based on its conjugate inverse-gamma posterior, and (ii) the optional use of the invariant treatment parametrisation introduced by Hahn et al. (2020), which requires additional Gibbs updates for treatment-specific scaling parameters. These details support a more complete understanding and implementation of the full posterior sampling procedure.

The noise is modelled as $\varepsilon_i \sim \mathcal{N}(0, \sigma^2)$, with the error variance σ^2 assigned a scaled inverse-chi-squared prior:

$$\sigma^2 \sim \text{Inv-}\chi^2(\nu, \psi), \quad (25)$$

where ν denotes the degrees of freedom parameter and ψ the prior scale. We follow Chipman et al. (2010), setting $\nu = 3$ and choosing ψ so that the prior is centred around a rough estimate of σ^2 .

The variance of the error is sampled from its conditional distribution. Recall that the prior is $\sigma^2 \sim \text{Inv-}\chi^2(\nu, \psi)$, which corresponds to an inverse-gamma distribution with shape parameter $\frac{1}{2}\nu$ and scale parameter $\frac{1}{2}\nu\psi$. By conjugacy, the posterior for σ^2 is inverse-gamma with updated shape parameter $\frac{\nu+n}{2}$ and scale parameter $\frac{1}{2}(\nu\psi + \sum_{i=1}^n r_i^2)$, where $r_i = T_i^o - \hat{T}_i$ denotes the residual for individual i , computed using Equation (2). Detailed derivations and further discussion can be found in Gelman et al. (2013, Section 3.2 and 14.2).

We adopt the conventional binary treatment indicator A , coded as 1 for treated individuals and 0 for controls, to clearly communicate our model structure and causal assumptions. However, the proposed model can also accommodate the invariant parametrisation introduced by Hahn et al. (2020), which relies on a data-adaptive treatment coding scheme. Under the invariant parametrisation, the model is re-expressed as:

$$\log T(a) = f(x, \hat{e}(x)) + b_a \cdot \tau(x) + \varepsilon, \quad (26)$$

where $\varepsilon \sim \mathcal{N}(0, \sigma^2)$ and:

$$b_1 \sim \mathcal{N}(0, 1/2) \quad \text{and} \quad b_0 \sim \mathcal{N}(0, 1/2). \quad (27)$$

In this formulation, the CATE is given by:

$$\text{CATE}(x) = (b_1 - b_0)\tau(x). \quad (28)$$

To implement this approach, two additional update steps are included in the Gibbs sampler to sample b_1 and b_0 . Conditional on the prognostic and treatment effect forests, and σ , these updates correspond to standard linear regression updates. Specifically, a linear model where the response is given by $\log T - f(x, \hat{e}(x))$ and the design matrix has two columns (without an intercept), defined as $(A\tau(x), (1 - A)\tau(x))$.

S.2 Reversible jump MCMC for tree updates

This section provides technical details on the reversible jump Metropolis—Hastings updates used to sample tree structures and their associated parameters in our model. We consider three reversible jump moves: GROW, PRUNE, and CHANGE. Each move is selected with fixed prior probabilities P_{GROW} , P_{PRUNE} , and P_{CHANGE} . These moves enable efficient exploration of the joint posterior over tree structures \mathcal{T} and step height parameters \mathcal{H} by proposing local modifications to $(\mathcal{T}, \mathcal{H})$. We update $(\mathcal{T}, \mathcal{H})$ jointly using the reversible jump framework (Green, 1995). The proposed pair is denoted by $(\mathcal{T}^*, \mathcal{H}^*)$.

This section provides technical details on the reversible jump Metropolis—Hastings updates used to sample tree structures and their associated parameters in our model. We update the tree structure \mathcal{T} and step heights \mathcal{H} jointly using the reversible jump framework (Green, 1995). We denote the current tree by $(\mathcal{T}, \mathcal{H})$ and the proposed tree by $(\mathcal{T}^*, \mathcal{H}^*)$. We consider three reversible jump moves: GROW, PRUNE, and CHANGE, selected with fixed prior probabilities P_{GROW} , P_{PRUNE} , and P_{CHANGE} . These moves enable exploration of the posterior by proposing local modifications to $(\mathcal{T}, \mathcal{H})$.

This section is organised as follows:

- We begin with a brief recap of the model setup and prior specification.
- We then provide a detailed derivation of the acceptance ratio for the GROW move, which involves a change in model dimensionality.
- Finally, we explain how the acceptance ratios for the PRUNE and CHANGE moves follow from similar principles.

An overview of the steps involved in a single-tree reversible jump update is given in Algorithm 2.

S.2.1 Recap of model setup and prior specification

We model the log-transformed survival times as a noisy sum of regression trees:

$$\log T_i = \sum_{j=1}^m g(X_i; \mathcal{T}_j, \mathcal{H}_j) + \varepsilon_i, \quad \varepsilon_i \sim \mathcal{N}(0, \sigma^2), \quad (29)$$

where m denotes the number of trees, \mathcal{T}_j is the tree structure, and \mathcal{H}_j is the set of step height parameters for the j -th tree.

We place independent priors on each pair $(\mathcal{T}_j, \mathcal{H}_j)$. The prior on the tree structure \mathcal{T} , originally proposed by Chipman et al. (1998), is defined as follows:

1. Start with a single root node.
2. A leaf node at depth d is split with probability

$$\rho_d := \frac{a}{(1+d)^b}, \quad (30)$$

where $a \in (0, 1)$ and $b \geq 0$ are hyperparameters.

3. The splitting variable is chosen uniformly at random from the available predictors.
4. The split point is chosen uniformly from the observed values of the selected variable.

The prior on the step height parameters \mathcal{H} , including any auxiliary parameters (e.g., local shrinkage parameters), is denoted by $p_{\mathcal{H}}(\mathcal{H} \mid \mathcal{T})$. Details can be found in Section 3.2.

Posterior updates for $(\mathcal{T}, \mathcal{H})$ are based on the residuals derived from the current model fit. For the j -th tree, these are given by:

$$\mathcal{R}_j := \log T^o - \sum_{J \neq j} f(X; \mathcal{T}_J, \mathcal{H}_J), \quad (31)$$

where T^o denotes the observed or imputed survival times after data augmentation.

S.2.2 The GROW move

When a GROW move is selected with probability P_{GROW} , the algorithm proposes to expand the current tree by splitting one of its terminal nodes (a leaf) into two new child nodes. This move increases the dimension of the parameter space and therefore requires a reversible jump step to ensure correct posterior exploration. The split is performed by selecting a valid splitting rule—that is, a covariate and a split point—which partitions the observations within the chosen parent node.

Consider a tree with three terminal nodes and corresponding step heights h_1, h_2, h_3 , as illustrated on the left side of Figure 8. Suppose we select the third leaf node (associated with h_3) for a GROW move. A splitting rule is applied to this node, yielding two new child nodes. These new regions inherit a subset of the observations from the parent node, based on the splitting rule, and are each assigned their own proposed step heights, denoted h'_3 and h'_4 . The resulting tree, shown on the right side of Figure 8, now contains four leaf nodes.

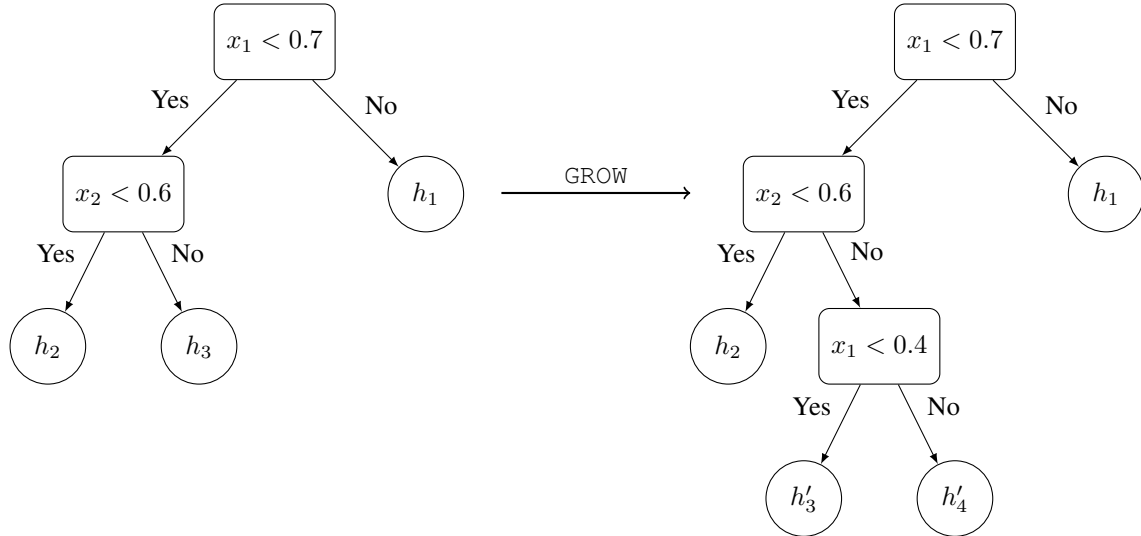


Figure 8: Example of a GROW move on a decision tree: the left tree is expanded by splitting the leaf node corresponding to h_3 . This yields two new leaves corresponding to step heights h'_3 and h'_4 .

The same transition can be viewed in the covariate space in Figure 9. The left square represents the region before the split (corresponding to h_3) and the right square shows the refined partition into h'_3 and h'_4 . This diagram offers geometric intuition for how the GROW move expands the parameter space by refining the partition of the covariate domain.

Let \mathbb{P} denote the parent node being split, which has associated parameters $(h_{\mathbb{P}}, \theta_{\mathbb{P}})$, where $\theta_{\mathbb{P}}$ represents local auxiliary parameters. For example, under the horseshoe prior with auxiliary variables (see Equation (16)), we have $\theta_{\mathbb{P}} = (\lambda_{\mathbb{P}}^2, \nu_{\mathbb{P}})$. The GROW move proposes two new sets of parameters for the child nodes: $(h_{\mathbb{L}}, \theta_{\mathbb{L}})$ and $(h_{\mathbb{R}}, \theta_{\mathbb{R}})$, where \mathbb{L} and \mathbb{R} denote the left and right child nodes as determined by the splitting rule.

These proposed values are drawn from pseudo Gibbs proposal distributions, as described in Section 4.2. The proposals are informed by the current parameters within the tree and the observed data: new values for the

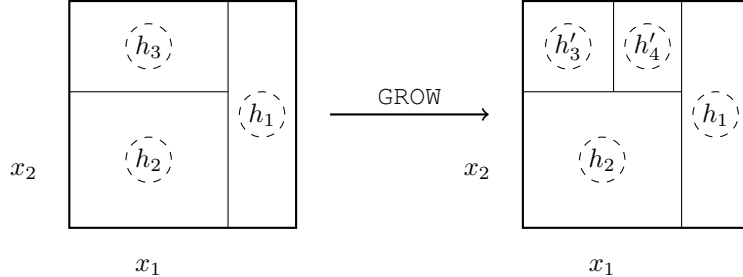


Figure 9: Illustration of a GROW move: the left panel shows the original covariate partition, and the right panel shows the updated partition with one additional split and two new step heights.

step heights and local parameters are generated from conditional distributions influenced by those of the parent node. While this resembles a Gibbs sampler, it is not a true one — the parent node’s parameters cannot be directly sampled since the node is replaced by two new children. This is not problematic as the Metropolis-Hastings acceptance step guarantees that the Markov chain targets the correct posterior, thereby ensuring convergence to the stationary distribution. The overarching goal is to construct proposals that are both informed and efficient.

We now derive the reversible acceptance ratio r_{GROW} for a GROW move. Note that the acceptance probability is given by $\min\{1, r_{\text{GROW}}\}$. The general framework for deriving the reversible jump acceptance ratio is outlined by Green (1995). Following this approach, the acceptance ratio builds on the Metropolis—Hastings formulation, as applied to tree-based models by Chipman et al. (2010), and incorporates both the proposal densities of the leaf parameters and the determinant of the Jacobian associated with the parameter transformation. A comprehensive overview of how to derive acceptance ratios for non-reversible updates in standard BART is provided by Kapelner and Bleich (2016).

We must satisfy the dimension-matching condition introduced by Green (1995) to perform a valid reversible jump move. Suppose we split a leaf node with associated parameters $(h_{\text{P}}, \theta_{\text{P}})$ into two child nodes with new parameters $(h_{\text{L}}, \theta_{\text{L}})$ and $(h_{\text{R}}, \theta_{\text{R}})$. We can interpret the parent node as having already been split, but with the child nodes initially inheriting the same values as the parent. This construction yields the same conditional posterior distribution and facilitates a reversible proposal structure. A schematic overview of this matching is depicted in Figure 10. The Jacobian of the transformation is equal to one because the new parameters are randomly drawn using the pseudo Gibbs proposal mechanism.

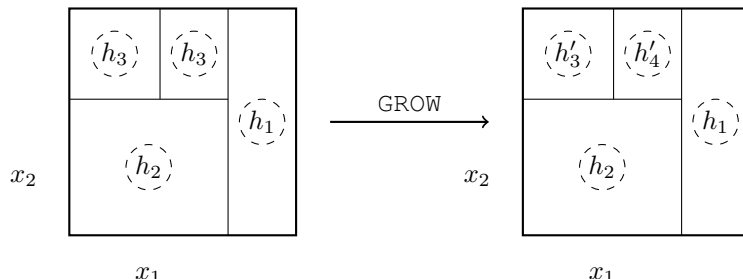


Figure 10: Illustration of the dimension-matching argument used in the GROW move. The left domain represents the initial tree configuration with a step height h_3 duplicated across two child regions. The right domain shows a proposed configuration where these regions are assigned distinct step heights h'_3 and h'_4 .

We derive the acceptance ratio r_{GROW} for a GROW move. This ratio compares the probability of proposing and

accepting a move to a larger tree versus reversing that move. It is given by:

$$r_{\text{GROW}} = \frac{q((\mathcal{T}, \mathcal{H}) \rightarrow (\mathcal{T}_*, \mathcal{H}_*))}{q((\mathcal{T}_*, \mathcal{H}_*) \rightarrow (\mathcal{T}, \mathcal{H}))} \cdot \frac{p((\mathcal{T}, \mathcal{H}) | \mathcal{R}, \sigma^2)}{p((\mathcal{T}_*, \mathcal{H}_*) | \mathcal{R}, \sigma^2)}, \quad (32)$$

where $q(\cdot \rightarrow \cdot)$ denotes the transition probability between tree states, and $p(\cdot | \mathcal{R}, \sigma^2)$ is the conditional posterior distribution given the residuals and noise level.

By applying Bayes' rule to the posterior terms, we rewrite the ratio as:

$$r_{\text{GROW}} = \underbrace{\frac{q((\mathcal{T}, \mathcal{H}) \rightarrow (\mathcal{T}_*, \mathcal{H}_*))}{q((\mathcal{T}_*, \mathcal{H}_*) \rightarrow (\mathcal{T}, \mathcal{H}))}}_{\text{transition ratio}} \cdot \underbrace{\frac{\mathcal{L}(\mathcal{R} | \mathcal{T}, \mathcal{H}, \sigma^2)}{\mathcal{L}(\mathcal{R} | \mathcal{T}_*, \mathcal{H}_*, \sigma^2)}}_{\text{likelihood ratio}} \cdot \underbrace{\frac{p(\mathcal{T}, \mathcal{H})}{p(\mathcal{T}_*, \mathcal{H}_*)}}_{\text{prior ratio}}, \quad (33)$$

where \mathcal{L} is the likelihood of the residuals (see Equation 14), and $p(\mathcal{T}, \mathcal{H})$ denotes the joint prior over tree structure \mathcal{T} and step height parameters \mathcal{H} .

The likelihood only changes for observations in the node being split. For all other observations, the likelihood remains the same. As a result, the likelihood ratio simplifies to:

$$\frac{\mathcal{L}(\mathcal{R} | \mathcal{T}, \mathcal{H}, \sigma^2)}{\mathcal{L}(\mathcal{R} | \mathcal{T}_*, \mathcal{H}_*, \sigma^2)} = \frac{\prod_{i \in \mathbb{P}} \mathcal{N}(\mathcal{R}_i | h_{\mathbb{P}}, \sigma^2)}{\prod_{i \in \mathbb{L}} \mathcal{N}(\mathcal{R}_i | h_{\mathbb{L}}, \sigma^2) \cdot \prod_{i \in \mathbb{R}} \mathcal{N}(\mathcal{R}_i | h_{\mathbb{R}}, \sigma^2)}, \quad (34)$$

where \mathbb{P} is the parent node being split, and \mathbb{L} and \mathbb{R} are the resulting left and right child nodes. We write $i \in \mathbb{L}$ to denote that observation i falls into node \mathbb{L} under the tree partitioning.

The prior ratio decomposes into the ratio of the tree structure priors and the prior on the step heights:

$$\begin{aligned} \frac{p(\mathcal{T}, \mathcal{H})}{p(\mathcal{T}_*, \mathcal{H}_*)} &= \frac{p_{\mathcal{T}}(\mathcal{T})}{p_{\mathcal{T}}(\mathcal{T}_*)} \cdot \frac{p_{\mathcal{H}}(\mathcal{H} | \mathcal{T})}{p_{\mathcal{H}}(\mathcal{H}_* | \mathcal{T}_*)} \\ &= \frac{\rho_d(1 - \rho_{d+1})^2}{1 - \rho_d} \cdot \frac{p(h_{\mathbb{P}} | \theta_{\mathbb{P}}) p(\theta_{\mathbb{P}})}{p(h_{\mathbb{L}} | \theta_{\mathbb{L}}) p(\theta_{\mathbb{L}}) \cdot p(h_{\mathbb{R}} | \theta_{\mathbb{R}}) p(\theta_{\mathbb{R}})}, \end{aligned} \quad (35)$$

where d is the depth of the split node, and ρ_d is the depth-dependent internal node probability from the tree prior (see Equation (30)).

The transition ratio accounts for move probabilities, available node choices, and proposal densities:

$$\frac{q((\mathcal{T}, \mathcal{H}) \rightarrow (\mathcal{T}_*, \mathcal{H}_*))}{q((\mathcal{T}_*, \mathcal{H}_*) \rightarrow (\mathcal{T}, \mathcal{H}))} = \frac{P_{\text{GROW}}}{P_{\text{PRUNE}}} \cdot \frac{k^{-1}}{N_*^{-1}} \cdot \frac{q_{\text{PRUNE}}(h_{\mathbb{P}}, \theta_{\mathbb{P}})}{q_{\text{GROW}}(h_{\mathbb{L}}, \theta_{\mathbb{L}}) \cdot q_{\text{GROW}}(h_{\mathbb{R}}, \theta_{\mathbb{R}})}, \quad (36)$$

where k is the number of leaf nodes in the current tree, N_* is the number of eligible internal nodes (nog nodes) in the proposed tree, and q refers to the proposal distributions. We use the notation q_{MOVE} to denote the proposal distribution used in each move, which is typically constructed as a pseudo Gibbs draw informed by the current state and residuals.

S.2.3 The PRUNE and CHANGE moves

In a PRUNE move, a *nog* node (a parent node with exactly two children) is selected, and its children are removed. This corresponds to merging two adjacent subregions in the covariate space. The PRUNE move is the exact inverse of the GROW move. As a result, its reversible jump acceptance ratio r_{PRUNE} is the reciprocal of the acceptance ratio for the corresponding GROW move:

$$r_{\text{PRUNE}} = \frac{1}{r_{\text{GROW}}}. \quad (37)$$

To propose parameters for the resulting leaf node, we must construct a reverse mapping from the child parameters. Several strategies are possible, such as averaging the child values or restoring the original parent values. We adopt the latter: the `PRUNE` move reverts to the parameter values of the parent node prior to the corresponding `GROW` move.

The `CHANGE` move modifies the splitting rule of an internal node while keeping the tree structure and parameter dimension fixed. Since the number of parameters remains unchanged, the reversible jump acceptance ratio r_{CHANGE} includes a likelihood ratio, a proposal ratio, and a prior ratio for the step height parameters.

Suppose we propose new values $(h_{\text{L}*}, \theta_{\text{L}*})$ and $(h_{\text{R}*}, \theta_{\text{R}*})$ to replace the current parameters $(h_{\text{L}}, \theta_{\text{L}})$ and $(h_{\text{R}}, \theta_{\text{R}})$. The acceptance ratio becomes:

$$\begin{aligned} r_{\text{CHANGE}} &= \frac{\prod_{i \in \text{L}} \mathcal{N}(\mathcal{R}_i | h_{\text{L}}, \sigma^2) \prod_{i \in \text{R}} \mathcal{N}(\mathcal{R}_i | h_{\text{R}}, \sigma^2)}{\prod_{i \in \text{L}*} \mathcal{N}(\mathcal{R}_i | h_{\text{L}*}, \sigma^2) \prod_{i \in \text{R}*} \mathcal{N}(\mathcal{R}_i | h_{\text{R}*}, \sigma^2)} \\ &\times \frac{q_{\text{CHANGE}}(h_{\text{L}*}, \theta_{\text{L}*}) q_{\text{CHANGE}}(h_{\text{R}*}, \theta_{\text{R}*})}{q_{\text{CHANGE}}(h_{\text{L}}, \theta_{\text{L}}) q_{\text{CHANGE}}(h_{\text{R}}, \theta_{\text{R}})} \\ &\times \frac{p(h_{\text{L}} | \theta_{\text{L}}) p(\theta_{\text{L}}) p(h_{\text{R}} | \theta_{\text{R}}) p(\theta_{\text{R}})}{p(h_{\text{L}*} | \theta_{\text{L}*}) p(\theta_{\text{L}*}) p(h_{\text{R}*} | \theta_{\text{R}*}) p(\theta_{\text{R}*})}. \end{aligned} \quad (38)$$

We draw the proposed parameters conditionally on the current ones. Although their interpretation may shift under the new split, the Metropolis—Hastings acceptance step accounts for this and preserves posterior correctness.

S.3 Supplementary tables for simulation results

The tables below present full numerical results for the main simulation study. These values correspond to the bar plots shown in Section 5.2 of the main text and are included here for reference and completeness. They report RMSE, coverage, and average credible interval length for both CATE and ATE, across all methods and covariate dimensions.

p	Method	CATE			ATE		
		RMSE	Cover.	Len.	RMSE	Cover.	Len.
100	Causal Horseshoe Forest	0.565	0.805	1.480	0.071	0.997	0.379
	Causal Horseshoe Forest (CV)	0.526	0.906	1.995	0.091	0.991	0.422
	AFT-BART	0.590	0.418	0.685	0.077	0.961	0.325
1000	Causal Horseshoe Forest	0.569	0.755	1.361	0.088	0.969	0.379
	Causal Horseshoe Forest (CV)	0.547	0.899	2.018	0.102	0.972	0.431
	AFT-BART	0.618	0.315	0.528	0.198	0.597	0.395
5000	Causal Horseshoe Forest	0.488	0.790	1.258	0.124	0.902	0.401
	Causal Horseshoe Forest (CV)	0.483	0.905	1.927	0.131	0.912	0.443
	AFT-BART	0.633	0.318	0.563	0.419	0.126	0.498

Table 1: Simulation results for the **linear** treatment effect scenario. Each table reports RMSE, coverage, and average interval length for CATE and ATE. These values correspond to the bar plots shown in Figure 3 in Section 5.2.

p	Method	CATE			ATE		
		RMSE	Cover.	Len.	RMSE	Cover.	Len.
100	Causal Horseshoe Forest	0.578	0.790	1.471	0.093	0.991	0.431
	Causal Horseshoe Forest (CV)	0.551	0.895	1.992	0.141	0.930	0.480
	AFT-BART	0.606	0.412	0.692	0.092	0.963	0.375
1000	Causal Horseshoe Forest	0.574	0.753	1.371	0.104	0.960	0.420
	Causal Horseshoe Forest (CV)	0.560	0.894	2.035	0.140	0.938	0.478
	AFT-BART	0.629	0.324	0.554	0.231	0.540	0.431
5000	Causal Horseshoe Forest	0.490	0.793	1.272	0.131	0.895	0.424
	Causal Horseshoe Forest (CV)	0.487	0.910	1.956	0.141	0.904	0.470
	AFT-BART	0.658	0.311	0.579	0.457	0.112	0.519

Table 2: Simulation results for the **non-linear** treatment effect scenario. Each table reports RMSE, coverage, and average interval length for CATE and ATE. These values correspond to the bar plots shown in Figure 3 in Section 5.2.

S.4 Additional simulations

We show a number of additional simulations to investigate the performance of the proposed methodology in a wider variety of settings.

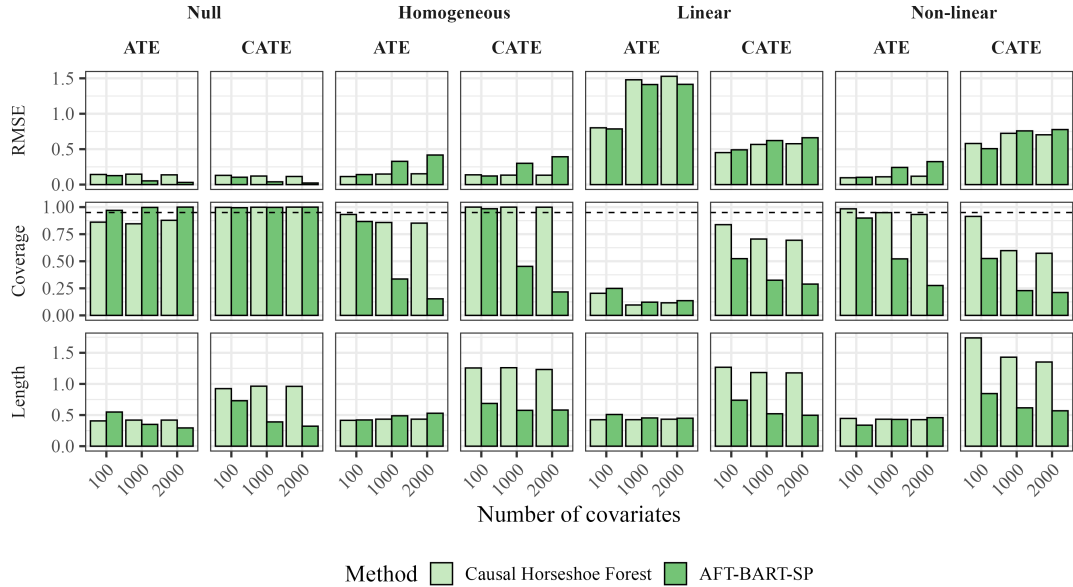


Figure 11: Comparison of Causal Horseshoe Forest and AFT-BART under block-correlated covariates. Results are shown for null, homogeneous, linear, and non-linear treatment effect scenarios across varying covariate dimensions p .

S.4.1 Highly correlated covariates

We consider the simulation set-up described in Section 5.1 with highly correlated covariates. We introduce correlations in blocks. This setup reflects scenarios where groups of features are strongly correlated, as is often the case in genetic studies.

Let $X = (X_1, \dots, X_p)$ be a vector of p covariates generated from a Gaussian copula:

$$G_{\Sigma}^{\text{Gauss}}(u) = \Phi_{\Sigma}(\Phi^{-1}(u_1), \dots, \Phi^{-1}(u_p)), \quad (39)$$

where Φ_{Σ} denotes the joint cumulative distribution function of a multivariate normal distribution with covariance matrix Σ , and Φ^{-1} is the standard normal quantile function. The covariance matrix Σ is constructed block-diagonally, with blocks of size 50, each having within-block pairwise correlations. We define a decaying correlation structure within each block:

$$\Sigma_{jk}^{(\text{block})} = \rho^{\frac{1}{2}|j-k|}, \quad j, k = 1, \dots, m, \quad (40)$$

where $\rho \in (0, 1)$ controls the within-block dependence strength. The blocks remain independent of each other.

We consider both the linear and non-linear heterogeneous treatment effect functions from Section 5.1. In addition, we include two homogeneous scenarios:

$$\begin{aligned} &(\text{Homogeneous}) \quad \tau(x_i) = 5, \\ &(\text{Null}) \quad \tau(x_i) = 0. \end{aligned} \quad (41)$$

The results are summarised in Figure 11. We observe that the prediction errors of the CATE are comparable to the setting with independent covariates. There is one exception: the RMSE of the ATE in the linear scenario is substantially higher. In this correlated setting, coverage levels for the ATE drop considerably, while the coverage for the CATE remains similar to the independent case, indicating more stable uncertainty quantification for individual treatment effects. In the homogeneous scenarios, both methods perform well. The Causal Horseshoe Forest achieves marginally lower RMSE and maintains approximately nominal coverage, while AFT-BART attain smaller CATE credible intervals, reflecting slightly tighter individual-level uncertainty bands.

S.4.2 Misspecification of the error

We next evaluate the robustness of the proposed method to error distribution misspecification in the AFT model. We repeat the original simulation setup and fit a Causal Horseshoe Forest using the default hyperparameter settings. Additionally, we fit two AFT-BART models: a semiparametric version and a non-parametric version. The latter is expected to be robust to model misspecification. We consider the same data-generating processes (linear and non-linear) with a fixed sample size of $n = 200$. The covariate dimensionality is varied over a wider range, including lower-dimensional settings.

We consider three different error distributions in the accelerated failure time (AFT) model. By varying the distribution of the error term ε , we induce different conditional distributions on the survival times. Specifically, we include the Gumbel and logistic. These corresponding respectively to the Weibull and log-logistic survival models. These distributions are widely used in survival analysis and reflect realistic event time patterns often observed in clinical data. For example, the log-logistic distribution can induce non-monotonic hazard functions, allowing for an initial increase in hazard followed by a decline, which better captures certain disease dynamics. In contrast, the Weibull distribution can represent both increasing and decreasing monotonic hazard rates depending on its shape parameter. Including these alternative error structures allows us to assess how each method performs under different, potentially misspecified, survival time assumptions.

We consider the following error distributions:

- **Gumbel distribution (Weibull model):**

$$\varepsilon \sim \text{Gumbel}(\mu, \beta). \quad (42)$$

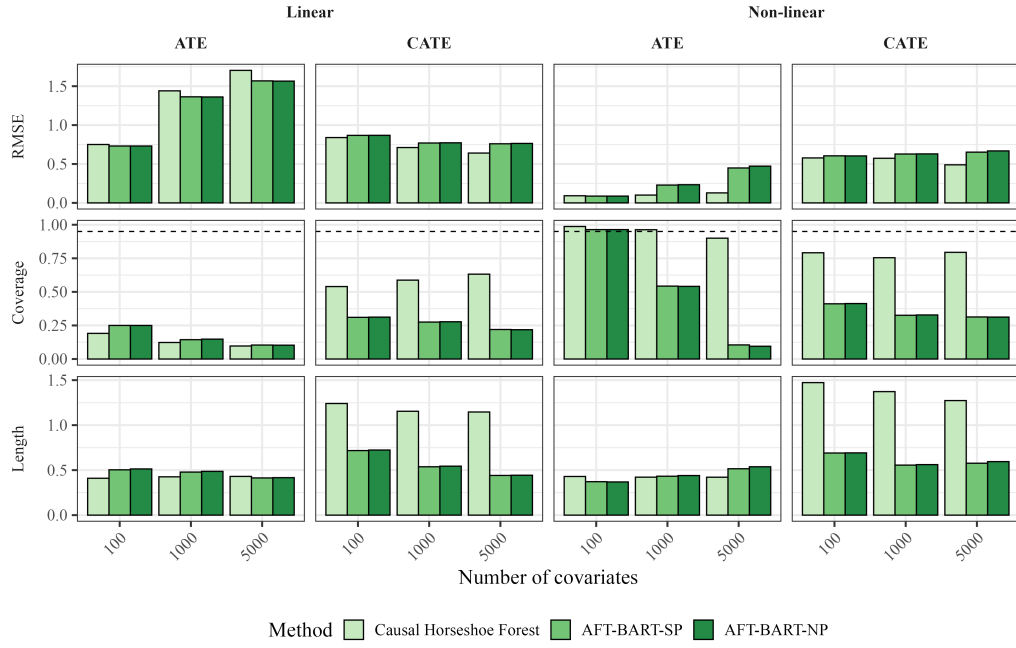
We set $\beta = \frac{3\sqrt{2}}{\pi}$ and $\mu = -\beta\gamma$, where $\gamma \approx 0.5772$ is the Euler–Mascheroni constant.

- **Logistic distribution (log-logistic model):**

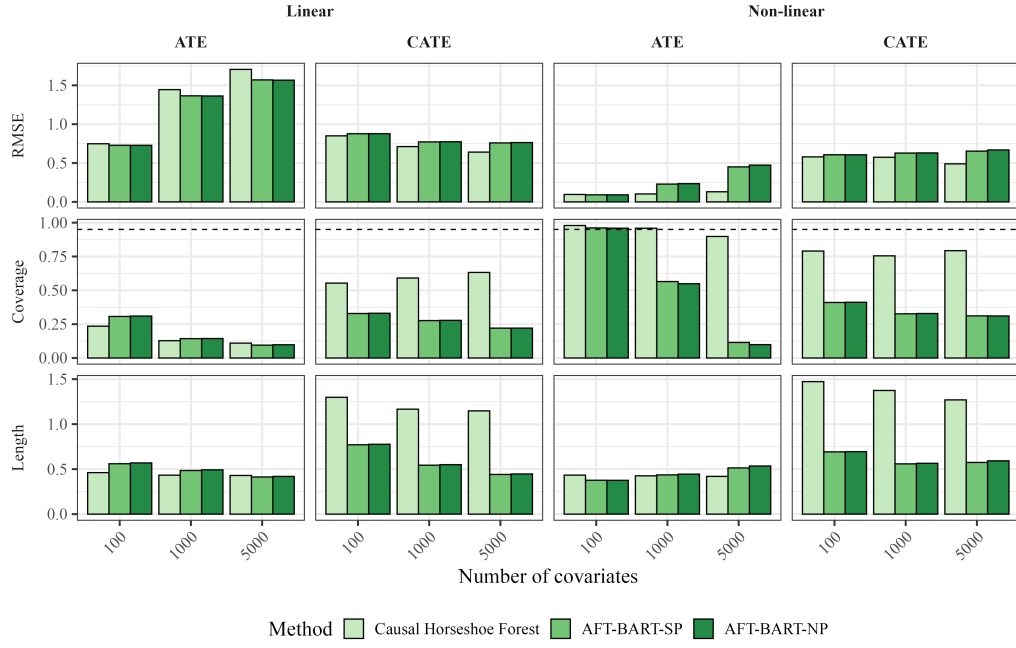
$$\varepsilon \sim \text{Logistic}(\mu, s). \quad (43)$$

We set $\mu = 0$ and $s = \frac{3}{\pi}$.

The results are presented in Figures 12a and 12b. Coverage drops for all methods under both the Gumbel and logistic error distributions. The Causal Horseshoe Forest consistently performs better. It maintains higher coverage for both the CATE and ATE, especially in non-linear settings. Even at $p = 5000$, coverage stays close to the nominal level. Causal Horseshoe Forest keeps CATE coverage around 80% in non-linear scenarios. In contrast, AFT-BART shows a sharp decline. Its coverage often falls below 60%, especially in high dimensions. The non-parametric AFT-BART is slightly more robust than its semiparametric counterpart. Still, it fails to maintain reliable coverage, particularly when treatment effects vary. These results mirror the patterns seen in the main simulations. They highlight the stability and adaptability of the Causal Horseshoe Forest across different error structures and under high-dimensional challenges.



(a) Gumbel error (Weibull survival time distribution)



(b) Logistic error (log-logistic survival time distribution)

Figure 12: Comparison of methods under two misspecified outcome models. Results are based on a sample size of $n = 200$, with varying covariate dimensions and both linear and non-linear treatment effect scenarios.

S.4.3 A dense model

We also consider a dense high-dimensional setting similar to Belloni et al. (2014) and Antonelli et al. (2022). In this scenario, the propensity score and prognostic functions are defined as:

$$\begin{aligned} e(x_i) &= \Phi(\beta^\top x_i), \\ f(x_i) &= \beta^\top x_i, \end{aligned} \tag{44}$$

where $\beta = (1, 1/4, 1/9, \dots, 1/p^2)$. For the treatment effect function, we consider two cases:

$$\begin{aligned} (\text{Homogeneous}) \quad \tau(x_i) &= 1, \\ (\text{Heterogeneous}) \quad \tau(x_i) &= 1 + x_{i1} - \frac{1}{2}x_{i2} + \frac{1}{3}x_{i3} - \frac{1}{4}x_{i4} + \frac{1}{5}x_{i5}. \end{aligned} \tag{45}$$

We set $n = 100$ and consider $p = 100, 300, 1000$, and variance of the noise at $\sigma^2 = 1$ and $\sigma^2 = 5$. This setup is not strictly sparse since none of the coefficients are exactly zero. However, it can be viewed as approximately sparse in the sense that a small number of leading covariates explain most of the confounding, while the remaining coefficients decay rapidly and contribute little to the overall bias.

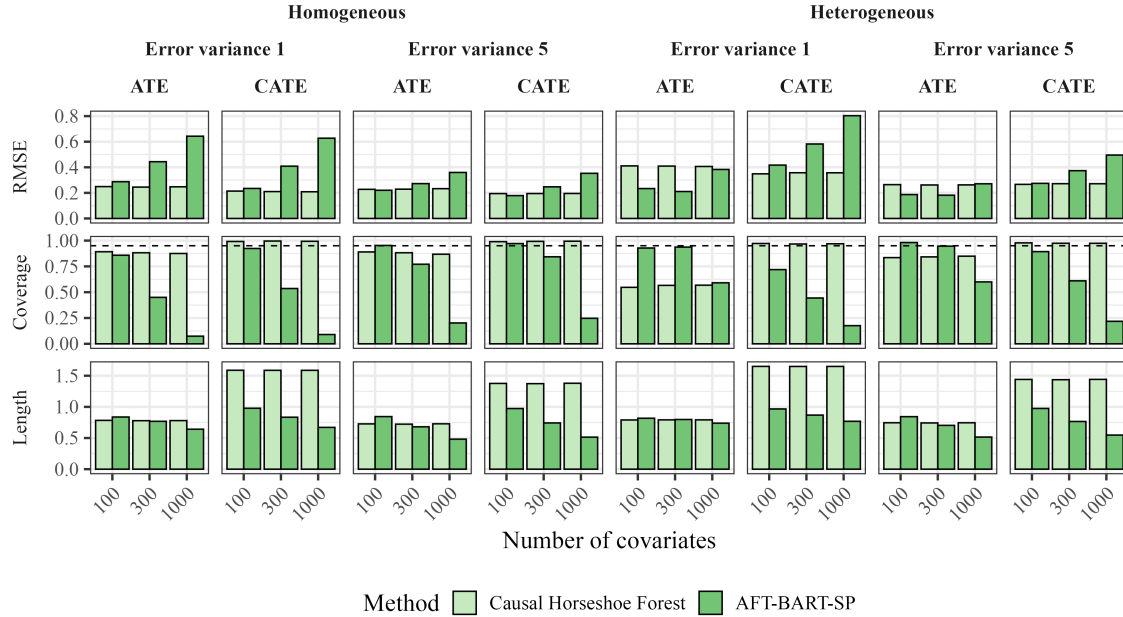


Figure 13: Performance of Causal Horseshoe Forest and AFT-BART under a dense high-dimensional setting, across varying p and error variances, for both homogeneous and heterogeneous treatment effects.

Figure 13 summarises the performance of Causal Horseshoe Forest and AFT-BART across different values of p and error variances under the dense model. We observe that Causal Horseshoe Forest benefits from higher noise in terms of prediction error in the heterogeneous scenario, while no clear effect is seen in the homogeneous case. AFT-BART, on the other hand, benefits from higher noise in both scenarios. In terms of coverage, Causal Horseshoe Forest outperforms AFT-BART in the homogeneous setting, particularly in higher dimensions. The picture is more nuanced in the heterogeneous scenario: Causal Horseshoe Forest attains appropriate levels of coverage for the CATE, whereas AFT-BART does not; for the ATE, this is vice versa, with AFT-BART showing higher coverage. Interestingly, AFT-BART appears to benefit from higher noise

with respect to coverage, whereas Causal Horseshoe Forest attains nominal coverage in both scenarios. The average treatment effect is captured relatively well by both methods. Causal Horseshoe Forest outperforms AFT-BART as the dimensionality increases.

S.5 Extra information PDAC analysis

This section provides additional details for the pancreatic ductal adenocarcinoma (PDAC) re-analysis presented Section 6. We list all clinical covariates included in the analysis (Table 3) and summarize key PDAC driver genes identified in the literature (Table 4). We report the results of cross-validated model selection using the C-index in Figure 14. We show a traceplot to assess MCMC convergence for the posterior standard deviation σ (Figure 15). Figure 16 shows the overlap in estimated propensity scores between treated and control groups.

Variable	Description
<i>Demographic information</i>	
age	Age of the patient at diagnosis (in years)
sex	Biological sex (0 = female, 1 = male)
<i>Tumor characteristics</i>	
grade	Histological tumor grade (1 = well, 2 = moderately, 3 = poorly, 4 = undifferentiated)
tumor.cellularity	Tumor cellularity as estimated by pathologist (numeric)
tumor.purity	Estimated tumor purity (0 = low, 1 = high)
absolute.purity	Tumor purity estimated using ABSOLUTE algorithm (numeric)
<i>Molecular and expression features</i>	
moffitt.cluster	Molecular subtype (0 = classical, 1 = basal-like)
meth.leukocyte.percent	Estimated leukocyte fraction based on DNA methylation (numeric)
meth.purity.mode	Tumor purity from methylation model (numeric)
<i>Staging and metastasis</i>	
stage	Nodal stage (0 = N0: no regional nodes, 1 = N1: nodal metastasis)
lymph.nodes	Number of lymph nodes examined (numeric)

Table 3: Overview of clinical covariates used in the PDAC data analysis.

Stefanoudakis et al. (2024)	Cicenas et al. (2017)	Takai & Yachida (2015)
<i>KRAS</i>	<i>BRCA1</i>	<i>ARID1A</i>
<i>TP53</i>	<i>BRCA2</i>	<i>ATM</i>
<i>CDKN2A</i>	<i>PALB2</i>	<i>RNF43</i>
<i>SMAD4</i>		<i>KDM6A</i>
		<i>PBRM1</i>
		<i>MLL3</i>
		<i>ARID2</i>
		<i>SF3B1</i>
		<i>BRAF</i>
		<i>NRG1</i>
		<i>RET</i>

Table 4: Genes identified as drivers in pancreatic ductal adenocarcinoma (PDAC) according to the literature.

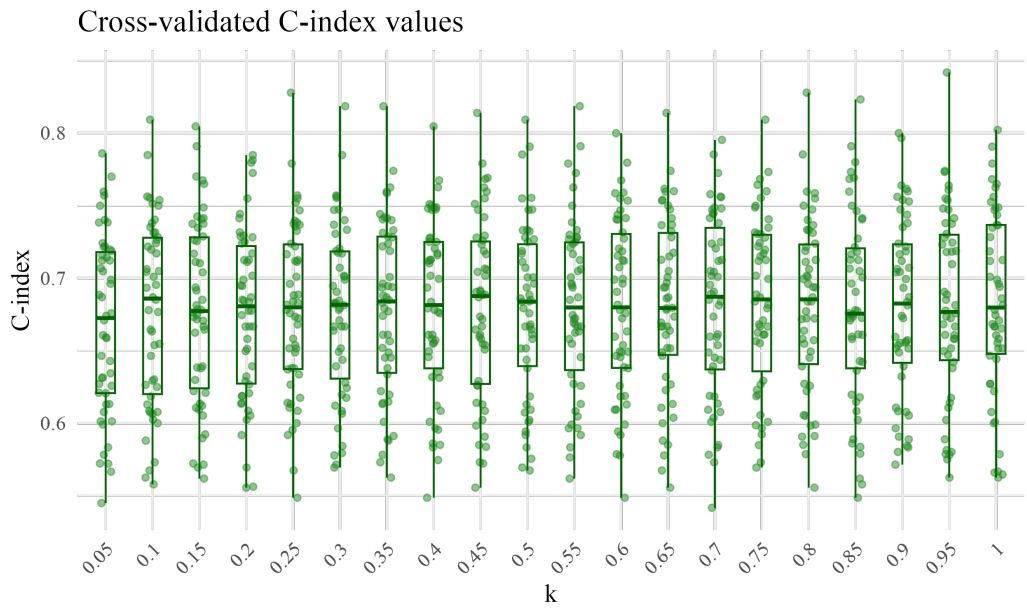


Figure 14: Stratified 10×5 cross-validated C-index values across different shrinkage values k .

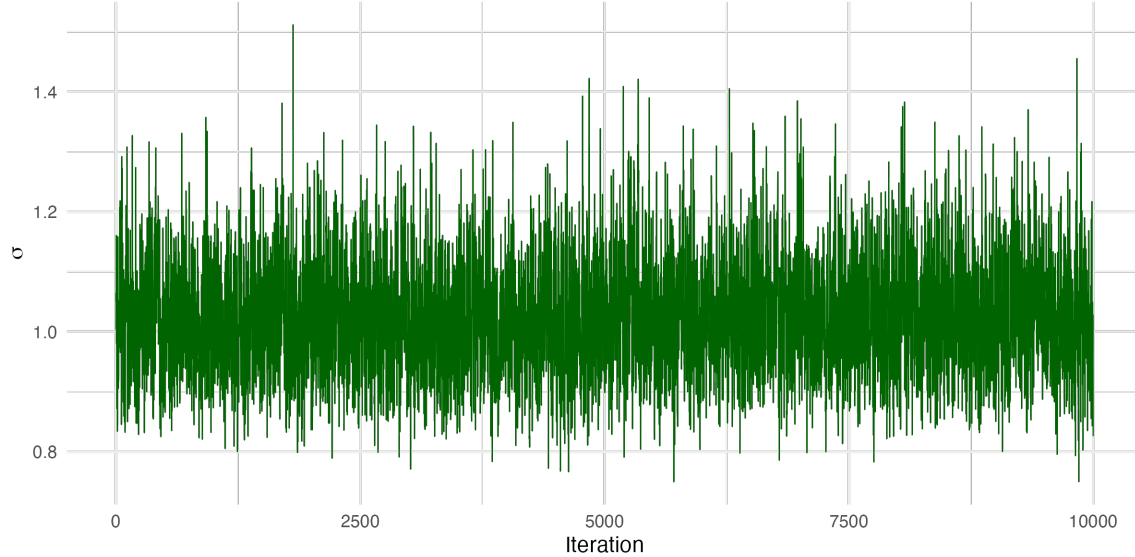


Figure 15: Traceplot of the posterior samples of σ , used to assess convergence of the Causal Horseshoe Forest sampler.

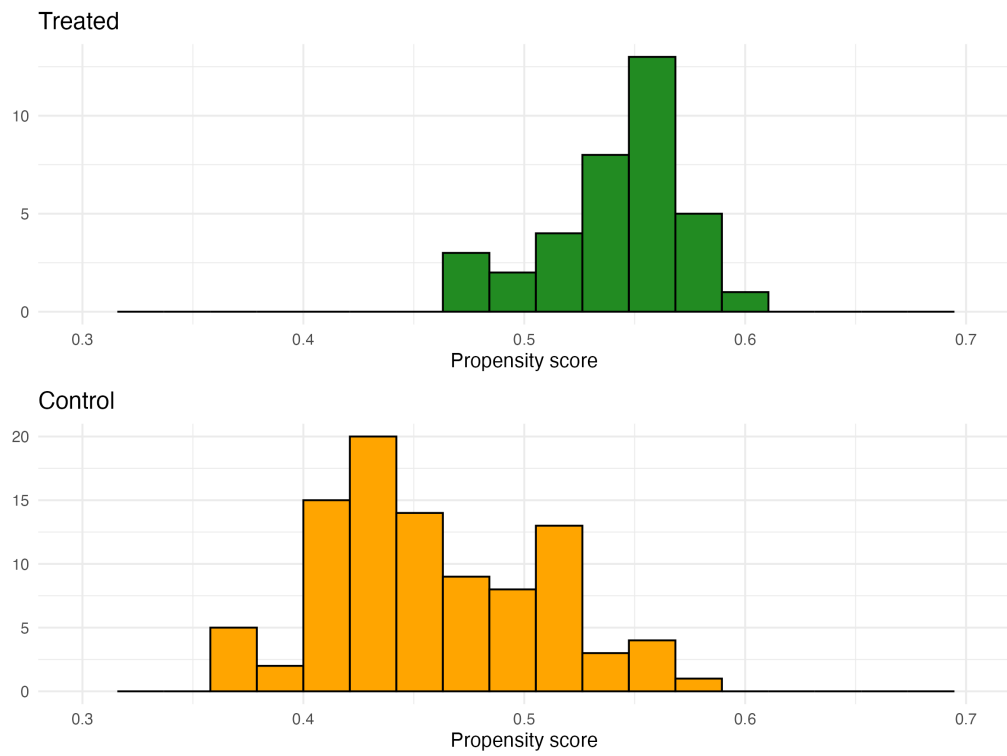


Figure 16: Histograms of estimated propensity scores for treated and control patients, showing the overlap in estimated treatment probabilities.

S.6 Exploratory landmark analysis of PDAC data

We conducted a preliminary landmark analysis on the PDAC data to explore the potential impact of immortal time bias. Two important caveats must be emphasised. First, we do not have detailed information on the exact timing of adjuvant radiation therapy initiation. We must therefore assume that at the chosen landmark time, patients classified as controls would not have subsequently received the treatment. Second, we applied our original model and estimands directly to the landmark cohort without formal adaptation to a rigorous landmark analysis framework. The results of this analysis should be interpreted with caution and viewed primarily as an exploratory sensitivity analysis, motivating further research rather than providing definitive causal conclusions.

The landmarking approach aims to mitigate immortal time bias by conditioning on survival up to a fixed time point. It ensures that all included patients are comparably at risk beyond the landmark time. This strategy has been advocated in the survival analysis literature as a pragmatic way to reduce immortal time bias (van Houwelingen and Putter, 2011). However, fully addressing this bias requires explicit modelling of time-dependent treatment assignment and joint survival-treatment processes. This was not possible with the available data.

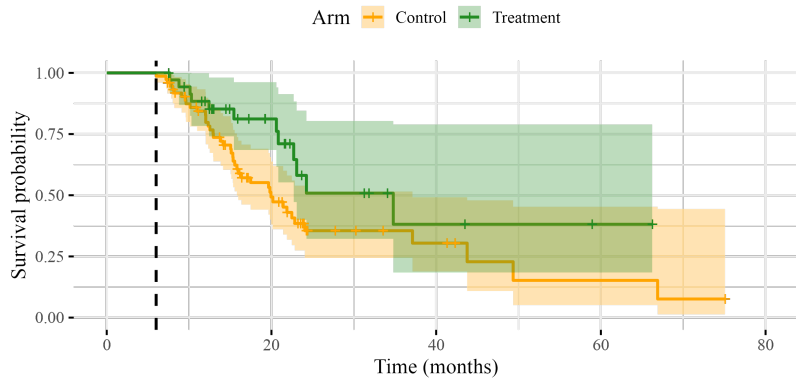


Figure 17: Kaplan–Meier survival curves for patients with PDAC after applying the 6-month landmark analysis. The vertical dashed line indicates the landmark time.

We set the landmark time at 6 months. Patients not at risk at this time point were excluded. This results in a sample of $n = 110$ patients, with 36 in the treatment group and 74 in the control group (based on the original sample used in the main analysis). The corresponding Kaplan–Meier survival curves are shown in Figure 17. We then re-estimated the causal effects using the Causal Horseshoe Forest approach described earlier.

The model achieved a concordance index of 0.75. The posterior mean ATE was estimated at approximately 0.55, with a 95% credible interval of (0.10, 0.98), as shown in Figure 18. Posterior distributions of the individual conditional average treatment effects are displayed in Figure 19. The estimated CATEs suggest a relatively homogeneous treatment effect across patients, although the wide credible intervals highlight the uncertainty due to the smaller sample size and reduced number of events after landmarking.

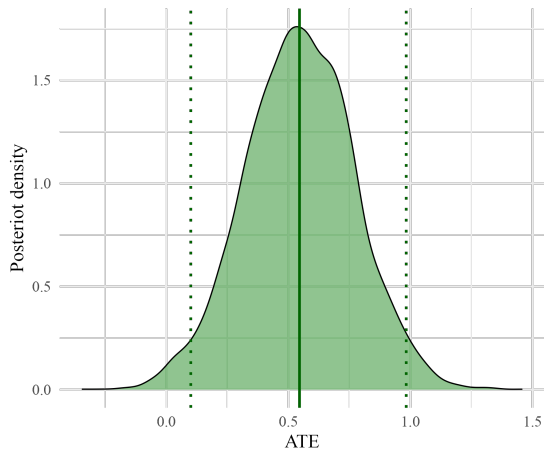


Figure 18: Posterior distribution of the ATE of adjuvant chemotherapy on overall survival in patients with PDAC after 6-month landmarking. The solid vertical line indicates the posterior mean, and dotted lines show the 95% credible interval.

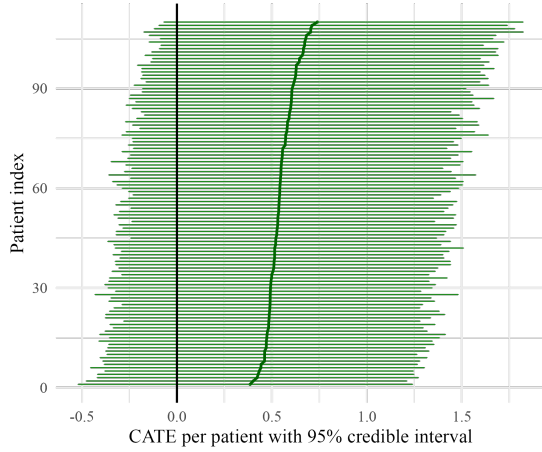


Figure 19: Posterior means and 95% credible intervals for individual CATEs under adjuvant chemotherapy in patients with PDAC after 6-month landmarking. Patients are sorted by estimated CATE.

The landmark analysis suggests a positive average treatment effect after accounting for potential immortal time bias. The estimated effect is smaller than in the main analysis. This suggests that immortal time bias may have inflated the treatment effect observed previously. The interpretation of this analysis crucially depends on the assumption that all patients would have had the opportunity to receive and complete adjuvant radiation therapy within one year after surgery. Future work incorporating explicit time-dependent treatment modelling is warranted to rigorously evaluate this potential bias.